NASA TECHNICAL TRANSLATION

NASA TT F-13,078

NASA TT F-13,078

THE EFFECT OF A SPIKE ON THE DRAG AND STABILITY OF BLUNT BODIES IN SUPERSONIC FLOW

Carlos Zorea (Zaritzky)

Thesis for the Degree of Master of Science,
Submitted to the Senate of the Technion,
Israel Institute of Technology,
Haifa, September 1969.

NATIONAL AERONAUTICS AND SPACE ADMINISTRATION
WASHINGTON, D. C. 20546 SEPTEMBER 1970

THE EFFECT OF A SPIKE ON THE DRAG AND STABILITY OF BLUNT BODIES IN SUPERSONIC FLOW

Thesis for the Degree of Master of Science

by

Carlos ZOREA (ZARITZKY)

Submitted to the Senate of the Technion

ISRAEL INSTITUTE OF TECHNOLOGY

Haifa, September 1969

TABLE OF CONTENTS

ANNOTATION

The study was carried out under the supervision of Assoc. Prof. Dr. J. Rom, at the Department of Aeronautical Engineering.

The author wishes to express his sincere gratitude to Assoc. Prof. Dr. Rom for his invaluable guidance and help in this study.

The author also wishes to thank:

The Direction of the Scientific Department of the Ministry of Defense for approving and financing the research.

Mr. Ben Tzion Naveh and Asher Sigal for their advice and help, and the Laboratory Staff of the Department of Aeronautical Engineering.

LIST OF SYMBOLS

a	-	diameter of spike
C_L	-	lift coefficient $\left(\frac{L^*}{\frac{1}{2}\rho V^2 S}\right)$
C_M	-	pitching moment coefficient $\left(\frac{M^*}{\frac{1}{2}\rho V^2 SD}\right)$
C_D	-	drag coefficient $\left(\frac{D^*}{\frac{1}{2}\rho V^2 S}\right)$
D	-	diameter of body
D_N	-	twice radius of blunt nose body
D*	-	drag
K	-	$2\sqrt{M^2-1}\ \mathrm{tg}\ \theta_c$
L	-	length of spike
L*	-	lift
M	-	Mach number
M*	-	pitching moment
P	-	pressure
$\frac{\Delta P}{q}$	-	dimensionless pressure rise (across conical shock wave)
q	-	$(\frac{1}{2}\rho V^2)$ dynamic pressure
R, r	-	radius
Re_d	-	Reynolds number, based on diameter
Re_f	-	Reynolds number, based on length of spike to its shoulder
S	-	reference area
X_{cp}	-	center of pressure distance (measured from base)
a	-	angle of attack
γ	-	cone angle of standing-water region
$\theta_{1/2}$	-	half of spike vertex angle
θ_c	-	solid angle of cone

/2*

/3

* Numbers in margin indicate pagination in the foreign text.

ρ - air density

ε - correction function

SUBSCRIPTS

b - base

Crit - critical

max - maximum

n - nose

LIST OF TABLES

/4

LIST OF TABLES (contd.)

ABSTRACT

In many aerodynamic configurations a blunt nose must be used. This causes the aerodynamic drag to be large, especially at supersonic speeds. It was previously proposed that the drag of a blunt nose body be reduced by means of a spike. Some results on basic configurations at well defined flow conditions are available [16 - 32] but there is less information on effects of the spike on the stability and on general design criteria using a spike.

The objectives of this investigation were as follows:

1. Drag reduction measurement for blunt nosed bodies as a function of spike length.

2. Determination of optimal spike lengths for supersonic Mach numbers.

3. Determination of spike's influence of the flow field.

4. Determination of spike's effect on the stability and lift of the blunt nosed body.

5. Reynolds and Mach numbers effects.

6. Development of a semiempirical method to evaluate the optimal spike length.

The experiments were carried out in the supersonic No. 7 tunnel at the Technion at Mach numbers of 1.5 and 2.25. The configuration chosen was a 1.5 fineness ratio nose and a hemispherical nose.

The following conclusions are obtained:

1. It is possible to reduce the drag of blunt nosed configurations by means of a spike at zero angle of attack by about 15% - 30%.

2. The relation between the spike length to nose radius is the most important parameter and governs the reduction of the body's drag.

3. The drag reduction that is obtained at zero angle of attack decreases with increasing angle of attack and disappears for an angle of 15°.

4. The blunt body's stability is not "spoiled" after the addition of the spike. In most cases it is improved.

5. The critical length of a spike is determined from the following relation:

$$\frac{L}{2\,r_n} = \frac{1 - \sin\theta_c}{2 \sin\theta_c}\left[1 + 2.5\left(\frac{a}{D}\right)^2 + 250\left(\frac{a}{D}\right)^4\right]$$

where

$$\theta_c = \arctan\left\{\left[9.44(M^2 - 1)^{0.0917}(0.0592 - 0.012\,M)^{1/1.69} \over Re_1^{0.0934}\right]\right\}$$

CHAPTER 1

DRAG AND STABILITY OF BLUNT BODIES IN SUPERSONIC FLOW

/7

It is known that narrowing and sharpening a blunt nose body decreases its drag. The aerodynamic designer wants to stay as close as possible to the elongated nose shape, because of its low drag. But in certain configurations there is a need for blunt nose bodies and for these there are two factors that influence and determine the value of the drag coefficient:

a. Shape - Ratio of nose radius to base radius.
b. Mach number - which decides the pressure jump across the detached shock wave and therefore also the pressure distribution of the body.

These two factors are assessed by two graphs taken from [1, 2]. The first shows how the drag coefficient varies as a function of the Mach number for the different nose body shapes, from a truncated cylinder to a parabolic peak of fineness ratio $\frac{lf}{R} = 8$.

It is evident from the graph that for these bodies the resistance of the drag coefficient increases with rising Mach number. For example, for a hemispherical shape, the drag coefficient is 0.67 at M = 1.5 and 0.80 at M = 2.25. The second graph shows the drag coefficient as a function of ratio r_n/r for r = 2.72. It can be seen from the graph that C_D is not affected at low r_n/r, but increases greatly at higher r_n/r. The problem of drag and the pressure distribution are discussed [3 - 15], which results were used for comparison with the author's tests.

If the length of the body is determined from previous considerations and the location of the center of gravity is also fixed, then blunt nose body causes a forward displacement of the center of pressure relative to the center of gravity. This creates a great pitching moment. Therefore in certain configurations a blunt nose body will cause drag as well as stability problems.

It was suggested some 15 years ago that drag on a blunt nose body can be reduced without impairing its stability and without interfering with the system it serves (e.g. homing head) by using a spike protruding from the center of the blunt shape. /8

CHAPTER 2

REVIEW OF PROPERTIES OF SPIKED BLUNT BODIES /9

2.1. Survey

The first studies concerning this subject were published by Moeckel in 1951 [15, 16]. Soon afterwards an extensive work started in this field in order to improve the drag performance of blunt configurations [17 - 23]. Moeckel attempted to solve the problem theoretically but his results do not agree with experimental data.

The other studies were experimental, like those of Mair, Jones and Stalder [19, 12, 18]. Mair used a hemisphere and a truncated cylinder ($M = 1.96$). Jones explored a cone terminating in a hemisphere ($M = 2.72$) and Stalder studied a hemisphere at $M = 1.75$ and $M = 2.67$. Concurrently the spike technique has been employed in the United Kingdom to solve problems in diffusers. This was done by Beastall and Turner who tested truncated cylinders of Mach numbers: 1.5, 1.6, 1.8 [20]. All the above experiments were performed at a zero angle of attack. Only later have other angles of attack been tried.

Hunt in the U.K. has examined a body similar to a hemisphere at Mach numbers 1.16, 1.81 and Kawasaki, Kawamoto and Shimizu in Japan ran experiments with a hemisphere and a truncated cylinder at Mach numbers of 2.5, 2.9, 3.8 [21, 23]. Lately Robinson came up with the technique of a spiked truncated cylinder to represent a parachute with zero porosity to solve the problem of parachute instability in the supersonic range.

Aerodynamic problems arising in conjunction with space flight and, in particular, with the re-entry problem, have induced several scientists concerned with hypersonic flow to consider spikes as a solution of heat-transfer problems [24 - 31].

2.2. Difficulties in the Use of Spikes for Minimal Drag

It has been found that a spiked termination of a blunt nose shape is accompanied by the following flow modifications: /10

a. For the same incoming flow conditions different flow fields are obtained at the spike shoulder as compared with a spike-less body.

b. Unsteady detachment zones in the vicinity of the spike produce pressure and heat transfer fluctuations at the nose.

c. Pressure hysteresis is a problem due to Mach number fluctuation of the incoming flow.

d. Attaching a spike increases the sensitivity of the pressure distribution, and of the drag and heat transfer with changes in angle of attack. Another difficulty of the lack of a theory or method of determining the optimal spike length and the range in which it is of advantage to use it in aerodynamic design.

2.3. Applications [32]

In the United States, spikes in blunt bodies have lately been used for different purposes in the supersonic and hypersonic regions. For example:

a. Use of spikes in hypersonic rocket tracks It is evident that at subsonic speeds the spike does not affect the drag of a blunt body, and that at high supersonic speeds its drag resembles that of a slender body. It is also clear that the spike weights less than a cone of comparable drag.

b. In the rocket used to orbit the Mercury space capsule This rocket has a blunt nose. A spike has been placed on it in order to lessen its drag in the supersonic and in the hypersonic ranges.

c. Arapaho "C" Test Vehicle A spike was used for improving the static stability at hyper- and supersonic velocities.

CHAPTER 3 /11

THE TEST EQUIPMENT

3.1. The Supersonic Wind Tunnel

All tests have been performed in the No. 7 wind tunnel at the Technion. This is a blow-down supersonic tunnel. The Mach number is adjusted by replacing of fixed cross-section nozzles. The description of the tunnel and its dimensions are given in Fig. 3 and general view in Fig. 5.

Air is supplied from a compressed air central system. The stagnation pressure is set by adjusting the supply valve. The test chamber cross section is 30×30 cm^2. The general view of the test cell and of the nozzles is given in sketch No. 4.

The stagnation temperature in the test chamber is about 0° C and cannot be directly adjusted since it depends on the compressed-air temperature and on the pressure drops across the control valve but the changes in the stagnation temperature are relatively small for short duration tests.

The angle of attack is determined by rotating of the model around the test chamber center in the vertical plane. The range of attack angles was, in our case, from -5° to +15°. A detailed description of the system is to be found in the "User's Manual" (see [33]).

3.2. Instrumentation and Testing System /12

3.2.1. Scales

Scales 3CLMD2 were used. They are capable of measuring the lift and drag and the pitching moment in the following ranges:

a. $L^*_{max} = 30$ kg.

b. $D^*_{max} = 20$ kg.

c. $M^*_{max} = 60$ kg-cm.

These scales are not temperature compensated, which caused hysteresis problems.

3.2.2. Auxiliary Instrumentation (see illustration No. 6)

We used a stroboscope for concurrent pulse transmission to the recording system and to the camera. The stagnation pressure being known, the Re number can be deduced for each photo. The flashing rate was 1 pulse/sec. This method is necessary, in particular, for tests with changing stagnation pressure.

3.3. The Models

3.3.1. Design of Models

The following factors were taken into account in designing of the models:

a. Maximum forces on scales. The models were designed after the scales were selected (see paragraph 4.2) and their maximum force and moment capacity was determined. The blunt-model drag was used as a basis in drag design of the other models.

b. The Length of the body. The length of the model was so determined that a part of its head and the spike would always appear in the window to allow for proper photographs to be taken. /13

c. Reynold's number. The Reynold's number was checked to determine conformance to our requirements.

3.3.2. Description of Models. The models are described in Fig. 7. They are made of aluminum and comprise a nose body, (one ogive-shaped, the other hemispherical) and of a rear cylindrical body with outside diameter D = 28 mm (Fig. 8). In the inside of the rear cylinder, an insert of insulating material (Durestos) was installed for shielding the scales from temperature changes. The nose body can be equipped with a variable length (L) spike.

The spike is also made of aluminum. The ratio of spike's diameter to body's diameter was 1/16 and the vertex angle of the spike was 20°.

The blunt nose body configurations tested differed by the L/D ratio of their spikes. The following L/D ratios were used:

TABLE 1. Configuration Designations

Configuration designation	L/D
000	0
005	0.5
010	1.0
015	1.5
020	2.0

3.4. Data Processing /14

The electrical readings are automatically recorded on a digital magnetic tape and also on analog recorders.

Data processing computation of aerodynamic coefficients was carried out with an Elliot 503 computer. The average gradients and zero lift angle were computed by the method of least squares and the program included corrections for the weight of the model and the deflections of the scales.

3.5. Photography

Schlieren and shadow photography was used. Three movie cameras (Ariflex special, Filler and standard Ariflex) were operated at 24 fps to 80 fps. Static photos were also taken, both ordinary and Polaroid. The methods and the equipment varied according to needs. Some tests were filmed by the color Schlieren method.

These photos were the only means used to interpret variations in the flow pattern and phenomena of high relative frequency.

3.6. List of Tests

Below is a list of tests performed and used for quantitative assessments (forces and moments) as well as for qualitative examinations of the flow pattern, etc.

TABLE 2. List of Tests

α	Re (1/cm)	Configu-ration	Run No.	Mach
0°	3.9×10^5	H 15	664	2.25
0°	7.2×10^5	H 00	645	"
0°	$6.1 \times 10^5 - 1.05 \times 10^6$	020	646	"
0°	$6.5 \times 10^5 - 1.08 \times 10^6$	010	647	"
0°	$7.7 \times 10^6 - 1.08 \times 10^6$	015	648	"
0°	$5 \times 10^5 - 1.15 \times 10^6$	000	649	"
0°	$3 \times 10^5 - 5 \times 10^5$	005	650	"
0°	$8.2 \times 10^5 - 1.18 \times 10^6$	010	651	2.25
0° - 4°	3.3×10^5	000	722	"

TABLE 2. Lists of Tests (Contd.)

α	Re (1/cm)	Configu-ration	Run No.	Mach
0° +5° - -5°	5×10^5 - 7×10^5 7×10^5	"	723	"
+10°; -5°	5.5×10^5	"	726	"
0°; 15°	5.5×10^5	"	733	"
0°	3.5×10^5	010	718	"
0°	4.7×10^5 - 8.8×10^5	"	719	"
+5°; -4°	3.8×10^5	"	721	"
0°; 15°	4.5×10^5	"	729	"
0°; 7.5°	$2.2 - 3.4 \times 10^5$	005	716	"
0°	$2.5 - 3.5 \times 10^5$	015	720	"
0°	4.6×10^5	000	782	1.5
0°; 4.5°	5×10^5	005	751	"
0° - 4°	4.8×10^5	010	753	"
-4.5°; 13°	4.5×10^5	010	785	"
0°	1.6×10^5 - 10^6	015	772	"
-4° - 15°	$1.8 - 5 \times 10^5$	015	772	"
-4.5°-15.2°	4.6×10^5	015	787	"

3.7. Accuracy

The error for each coefficient is given as a numerical increment for each coefficient and not as percentage.

Error	Coefficient
± 0.01	C_D
± 0.075	C_L
± 0.150	C_M

Corrections due to temperature changes were not made.

CHAPTER 4

FLOW AT ZERO ANGLE OF ATTACK /16

4.1. Flow Pattern

When there is no spike, or when the spike is very short, there is a strong detached shock wave ahead of the nose body. When the spike's length is increased until it comes into contact with the detached shock, the latter becomes a conical wave attached to the spike's tip. The conical wave is followed by a conical flow which borders with a mixing layer serving as the boundary of a standing water zone around the spike (see sketch A).

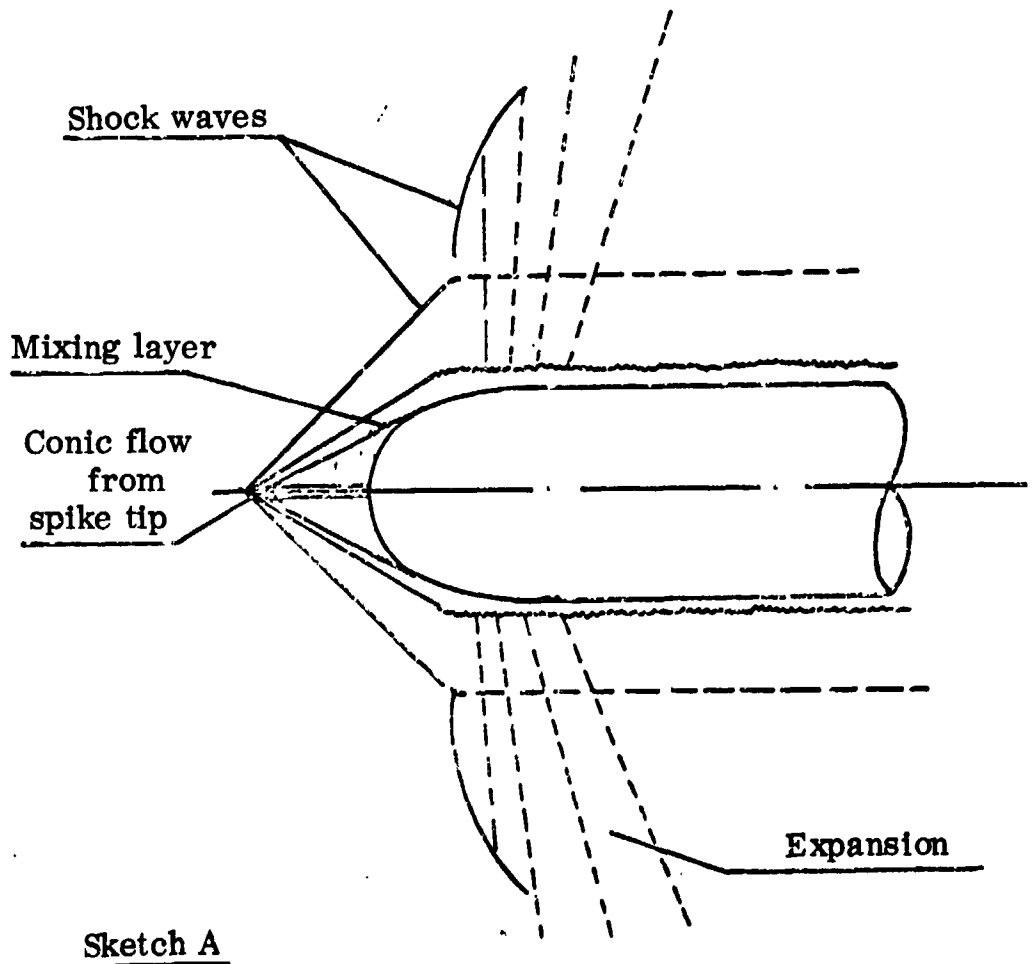

Sketch A

SHORT SPIKE

Increasing the spike's length up to its critical value elongates the mixing zone (between the conical flow and the standing water). It is evident from the tests that as the mixing zone becomes longer, the nose*detached wave becomes weaker. The conical flow becomes progressively smaller until a certain angle is reached (see sketch B) at which the conical flow's origin moves to the spike's shoulders.

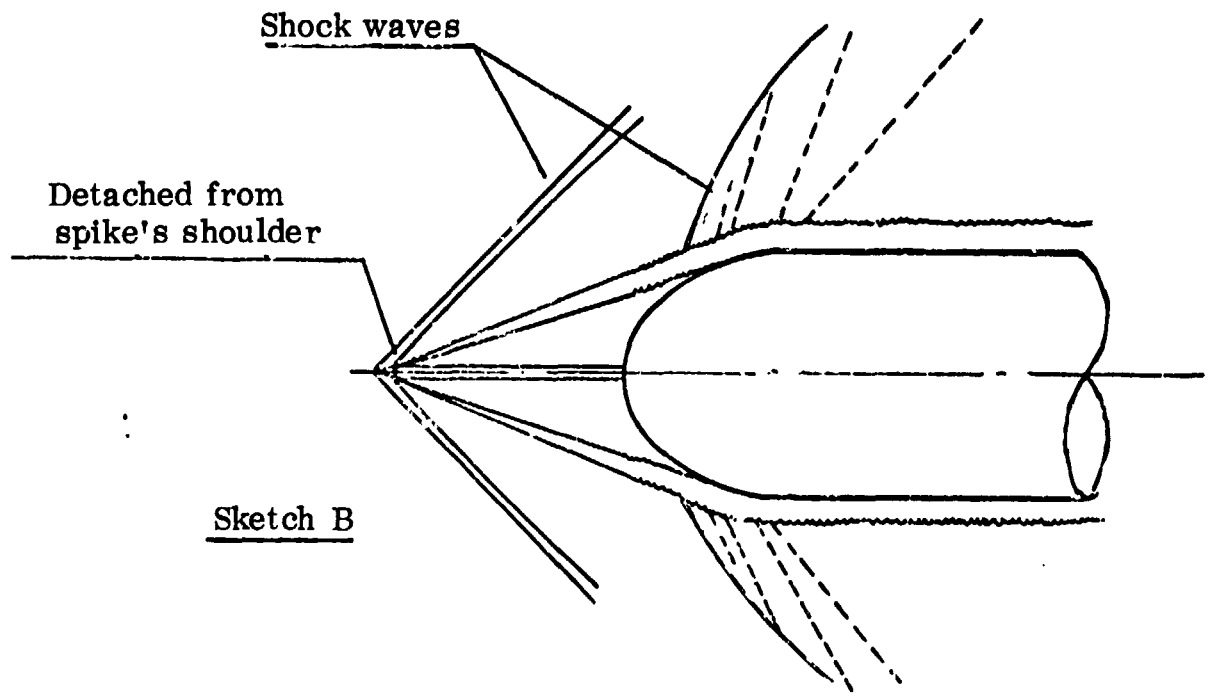

Sketch B

/17

Spike Somewhat Shorter than Critical Length

The boundary layer that becomes detached from the shoulder forms the edge of the conic flow. The separated boundary layer does not come into total contact with the blunt body (nose), which causes a shock wave to appear where the boundary layer swings around the nose. The detached shear layer serves as a mixing region between the conical flow and the standing-water zone.

When the spike exceeds a certain length (called critical) the separation point does not remain on the spike's shoulder, but suddenly jumps downstream (see sketch C).

At certain Mach and Reynolds numbers this separation is unstable and the separation point moves back and forth between the spike's shoulder and some point on the spike's surface (see Fig. 9).

Apparently this continuous shifting of the separation point is due to the fact that the separated boundary layer is still laminar at the spike, but as soon as it becomes turbulent before it reaches the separation zone, the shifting stops.

/18

*nose is used to distinguish from spike

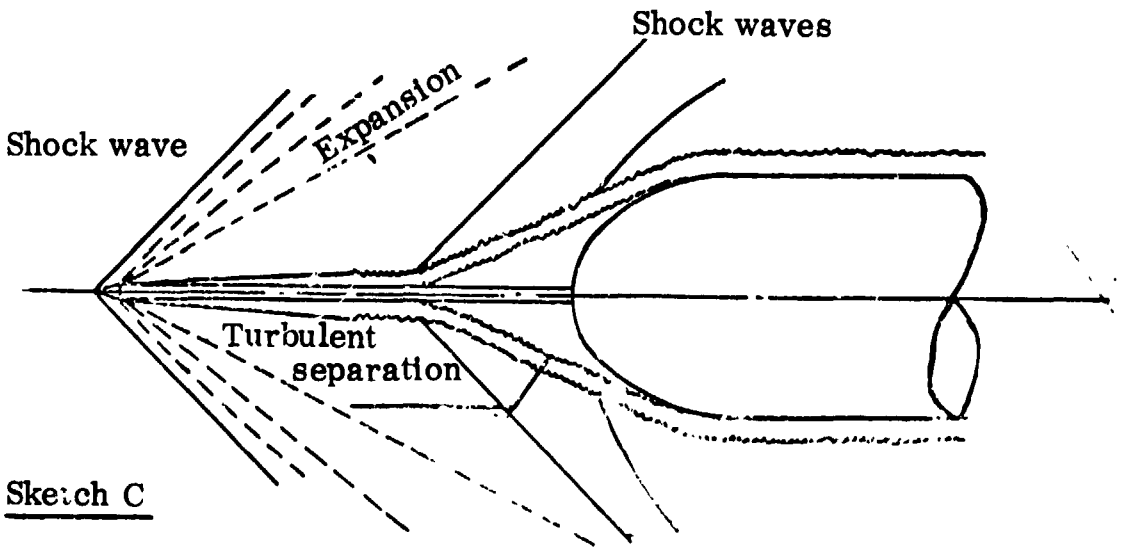

Sketch C

VERY LONG SPIKE

When the layer is laminar at the separation point, an increase in the Re number per unit length (at a constant M), increases the angle of flow separation and thus decreases the critical spike length. An increase in M with Re constant decreases the minimum flow separation angle, thus increasing the critical spike length. The same trend was found in earlier work (see [21] and [34]). It was proved in other studies that the standing water zone is far from being a stagnation zone.

4.2. Drag

Pressure measurements on the spike surfaces made previously by others show that maximum pressure is attained in the flow reattachment zone. Beyond the reattachment point the pressure drops due to flow expansion in the next part of the body, and therefore a blunt body with a spike cannot be regarded as a solid cone for the purpose of pressure distribution and drag coefficient determination.

In general, with increasing spike length the drag gradually decreases to a minimum at critical spike length. Then the drag undergoes a step increase and it can be expected that it will stay constant for configurations with very high $L/2r_n$ ratio. The changes in drag produced by changes in spike's length correspond to the flow pattern changes described above.

For short spikes the mixing zone starts from the spike's tip. For a certain spike length (shorter than critical) the mixing zone starts from the spike's shoulder rather than from its tip. This happens suddenly, on reaching the certain length. In the present tests, this happened, for example at $M = 2.25$ and $Re = 4.10^5$ (cm^{-1}) for a ratio $L/D = 0.5$ (see Fig. 10). This explains why for a certain L/D a discontinuity is to be expected in the drag coefficient (region A in the sketch). /19

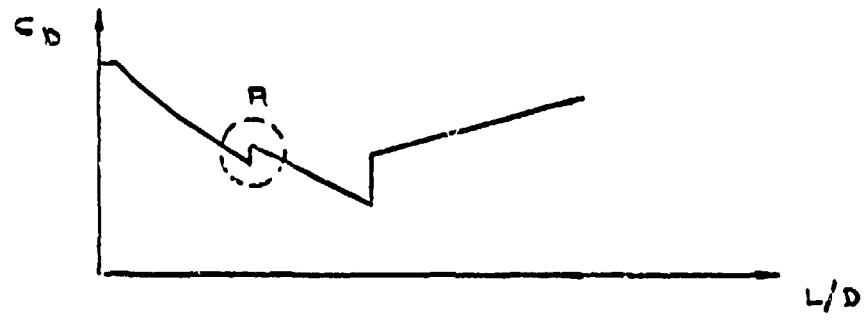

This happens because the opening angle of the mixing zone gets smaller with increasing spike length and the end of the mixing zone meets the shoulder. It is evident that for different spike tips the transformation will conform to the specific geometry, and therefore this phenomenon can be considered as being strictly local, without much influence on the general spike effect.

4.3. Tests at M = 1.5 and M = 2.25

Many of the present tests were performed for zero angle of attack (see Figs. 11 and 12) (see Sec. 4.6). The computed results together with the photographs have contributed to the understanding of the physics of the problem and assisted in forming a quantitative assessment of the drag coefficient. The drag coefficient as a function of L/D, appears in Figs. 13 and 14 for Mach numbers 1.5 and 2.25 in the range $Re = 1.6 \times 10^5 - 1.2 \times 10^6$ cm^{-1}.

CHAPTER 5

/20

THE CRITICAL LENGTH AND THE METHOD FOR ITS DETERMINATION

5.1. The Critical Length

Much was written on the interactions between a boundary layer and a shock wave, with most investigators considering two-dimensional flow, but these studies are not applicable to flow problems in the spike zone since in them boundary-layer thickness is great compared to the spike's diameter.

The critical length was found using the Donaldson [34] approach. This work deals with a flat plate, and it was found there that for some Re and boundary-layer state, the minimum pressure increases as a result of shock separation of the boundary layer.

If the separation of the boundary layer from a small-diameter spike is approached in a similar manner, it may be claimed that the conical shock wave, situated ahead of the separation point, represents a pressure causing the boundary layer separation at some [Mach] number and some flow pattern in the boundary layer.

The equilibrium can therefore be defined as follows:
The vertex of the separated flow cone is held at the spike's tip at a point determined by the pressure field existing ahead of the spike.

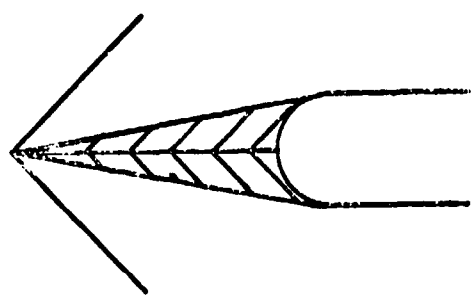

If the spike is lengthened into the zone of the standing water a more slender cone is formed.

As the cone becomes more and more slender, the pressure vise across the shock wave at the spike becomes smaller. At a certain length the pressure rise across the shock does not suffice for detaching the flow from the spike and the point of separation jumps from the spike's shoulder to the spike's body. /21

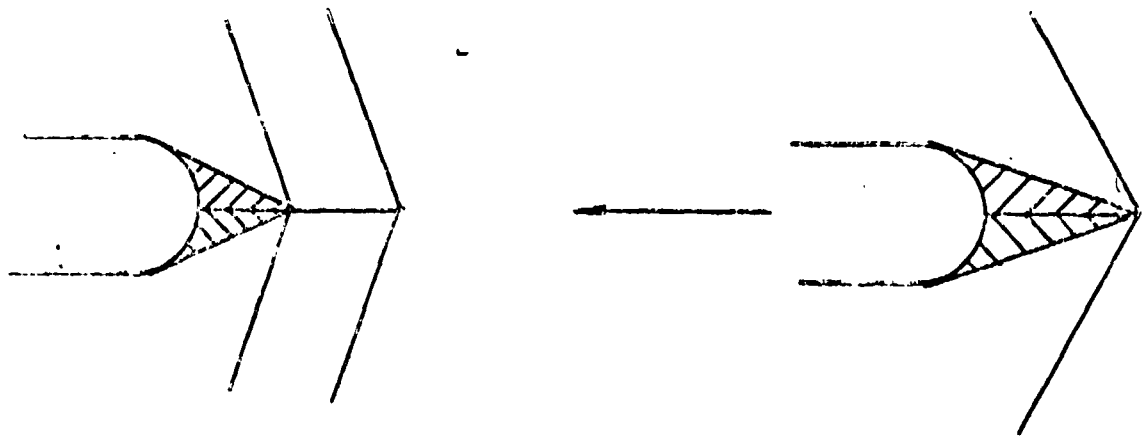

It was expected that the point of separation would continuously move along the spike as the latter's length increases, but as the separation point moves along the spike, the Re at it increases and the boundary layer changes from laminar to turbulent.

Under turbulent conditions a greater pressure rise across the shock is needed for separating the boundary layer. For this reason the separation point moves jumpwise along the spike and forms, by combining with the mixing zone, a standing-water cone with a larger opening angle; another shock wave is then formed ahead of this cone.

With reference to the above, the critical length of the spike can be defined as the length, any increment of which will cause the point of separation to jump from the spike's shoulder to some point at body.

It follows from the experiment and the above reasoning that when the spike is of critical length, the drag coefficient of the configuration is minimal, and hence further research should concentrate on methods for the determination of the critical length.

5.2. The Method of Determining the Critical Length /22

We start with the following assumptions:

a. Reference is had to a hemispherical or some similar shape*.

b. A very slender spike a/Dn0 ratio is used.

*A similar body is one composed of two radii, one of which corresponds to a hemisphere. The detached zone must be tangent to this segment.

c. In a configuration with a critical-length spike the cone of the standing water zone is tangential to the body (this assumption is only geometrically correct and is based on Schlieren photographs. This assumption cannot be used for drag computation).

d. The angle of the standing water is the solid angle which is defined by the conic flow tables for a given Mach number and Mach angle. In our Mach number range ($1.5 < M < 2.75$) we shall use the correlation given for cones in [35]:

$$\frac{\Delta p}{q} = \frac{0.705\ K^{1.69}}{M^2 - 1} \tag{1}$$

where

$$K = 2\sqrt{M^2 - 1}\tan\theta_c$$

The determination of the critical length involves the following:

a. Determination of critical length $(\frac{\Delta p}{q})_{crit}$ as a function of M and Ref., based on results of the present work and published data. The experimental points are plotted in Fig. 15 and were obtained for a spike-tip angle of 20°.

The family of curves correlating test points is described by the empirical formula (Fig. 15).

$$\frac{\Delta p}{q} = (0.0592 - 0.012\ M)\ Ref^{3/19} \tag{2}$$

The fact that the Reynolds number has a positive exponent shows $\frac{\Delta p}{q}$ and θ_c increase as Re increases and L/Dn decreases. This was in the present experiment and was also noted by others. /23

b. Having determined the value of $\frac{\Delta p}{q}$, θ_c is determined from assumption d (using the conic flow tables of Eq. (1)).

c. On the basis of assumptions a, b and c above, and from the following geometrical definitions:

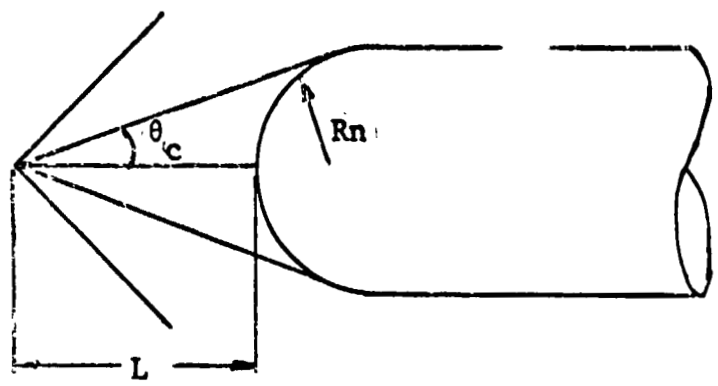

$$\frac{Rn}{L+Rn} = \sin\theta_c \qquad (3)$$

one easily obtains the ratio

$$\frac{L}{2Rn} = \frac{(1-\sin\theta_c)}{2\sin\theta_c} \qquad (4)$$

Eqs. (1) and (2) yield the following:

$$\theta_c = \arctan\left[\frac{M^2-1}{0.705}\,(0.0592-0.012\,M)\,Re_f^{\,3/19}\right]^{1/1.69}\left(\frac{1}{2\sqrt{M^2-1}}\right) \qquad (5)$$

Equations (4) and (5) define the solution, and facilitate the determination of L if M and Re_f are known.

Since the fact that a/Dn = 0 was accounted for in this derivation, we shall multiply the solution obtained by the correction function to take into account the effect of the spike's diameter. The empirical correction obtained from comparison with experimental results is given by (see Fig. 16): /24

$$f\left(\frac{a}{D}\right) = 1 + 2.5\left(\frac{a}{Dn}\right)^2 + 250\left(\frac{a}{Dn}\right)^4 \qquad (6)$$

This correction is valid up to a/Dn = 0.2.

Equations (4) and (6) yield the following expression for the critical length:

$$\frac{L}{Dn_{crit}} = \frac{1-\sin\theta_c}{2\sin\theta_c}\left[1 + 2.5\left(\frac{a}{Dn}\right)^2 + 250\left(\frac{a}{Dn}\right)^4\right] \qquad (7)$$

where θ_c is given by Eq. (5).

A computer program was prepared for obtaining $(L/Dn)_{crit}$ for a certain a/Dn and for our range of M and Re_f

The results appear in Figs. 17a through 17e.

The equations presented up to now are valid for the following conditions:

1. Ref = 2.5×10^4 - 3.5×10^5.
2. M = 1.5 - 2.75.
3. Hemispherical or similar nose body.
4. Slender spike (a/Dn up to 0.2).

Table 3 compares the results obtained by different investigators using present method.

TABLE 3. Comparision of Experimental Results with Estimates /25

$(Lc/2Rn)$ According to pres. method	$(Lc/2Rn)$ Empirical	$a/2Rn$	Re_x	M	Author
1.62	1.65	0 067	2.96×10^4	1.69	Mair (18)
1.50	1.50	0.100	2.02×10^5	2.67	Stalder (19)
1.82	1.87	0.200	3.15×10^5	1.81	Hunt (21)
2.03	2.00	0.200	1.12×10^5	1.81	Hunt (21)
1.51	1.50	0.067	5.2×10^4	1.81	Hunt (21)
1.25	1.27	0.081	2.5×10^5	1.50	Present work
1.30	1.27	0.081	2.8×10^5	2 25	Present work

It is evident from the table that the experimental results and those obtained by the present method are in satisfactory agreement.

CHAPTER 6

FLOW AT NONZERO ANGLE OF ATTACK /26

6.1. General

It has been known for a number of years that a spike at the nose of a blunt body is capable of reducing the supersonic drag at zero angle of attack. Only few investigators [21, 22] attempted to check whether this holds true also for non-zero angles of attack.

In the present work we wished to establish:

a. The effect of angle of attack on the drag coefficient.

b. The effect of angle of attack on the lift coefficient, the [pitching] moment coefficient and the center of pressure.

6.2. The Flow Pattern

The flow behavior at different angles of attack is described in sketches D, E and F. These describe the flow, based on information obtained by Schlieren shadow photographs. When the body is at some angle of attack the flow ceases to be symmetrical. Sketches D and E show that a change of a few degrees affects seriously the flow pattern.

The angle between the detached boundary layer and the free flow direction remains constant. Therefore the detached flow cone that starts from the spike stays in the direction of the flow. Due to this the portion sheltered by the cone decreases progressively with increasing in angle of attack and it is seen from graphs (Figs. 18 and 19) that at angle of attack of 15° half of the hemisphere remains unshielded. /27

When the spike is longer than critical (sketch F) the turbulent lift line changes the conic flow pattern which makes it necessary to treat this subject separately.

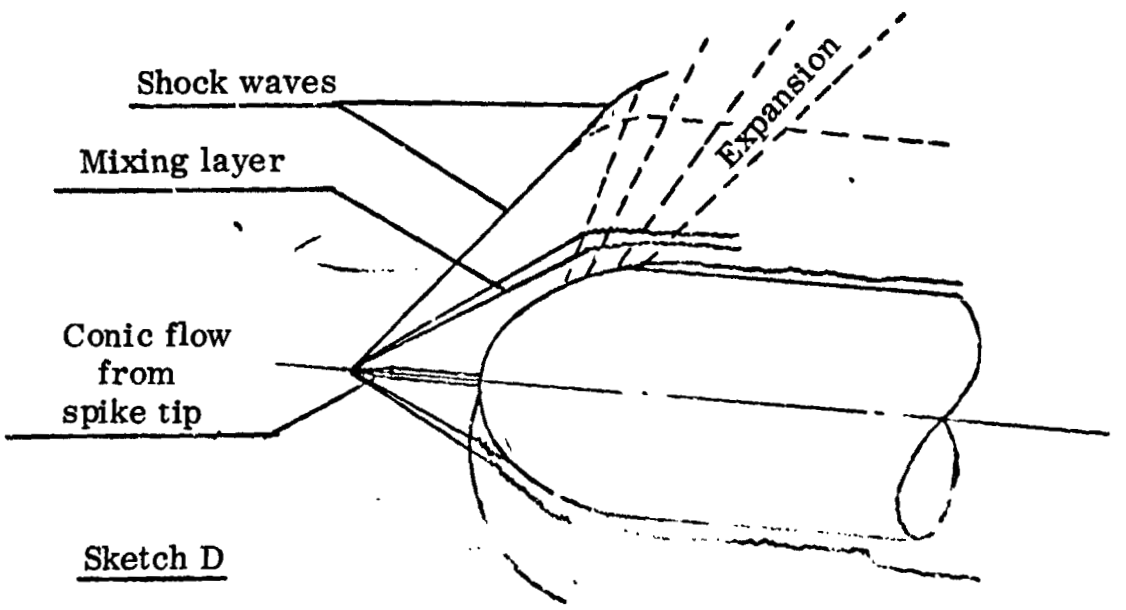

Sketch D

SHORT SPIKE

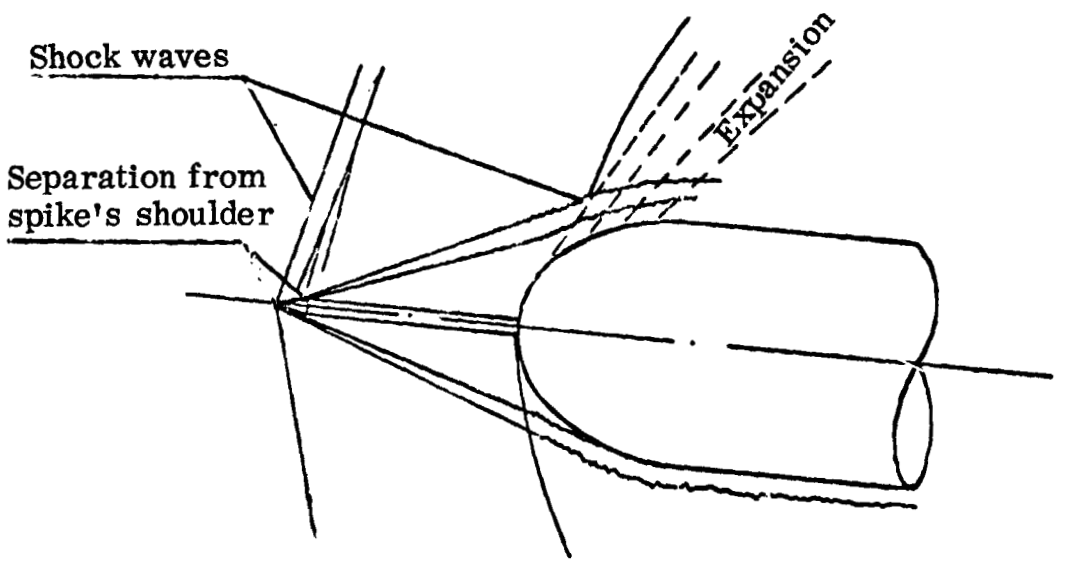

Sketch E

SPIKE SOMEWHAT SHORTER THAN CRITICAL

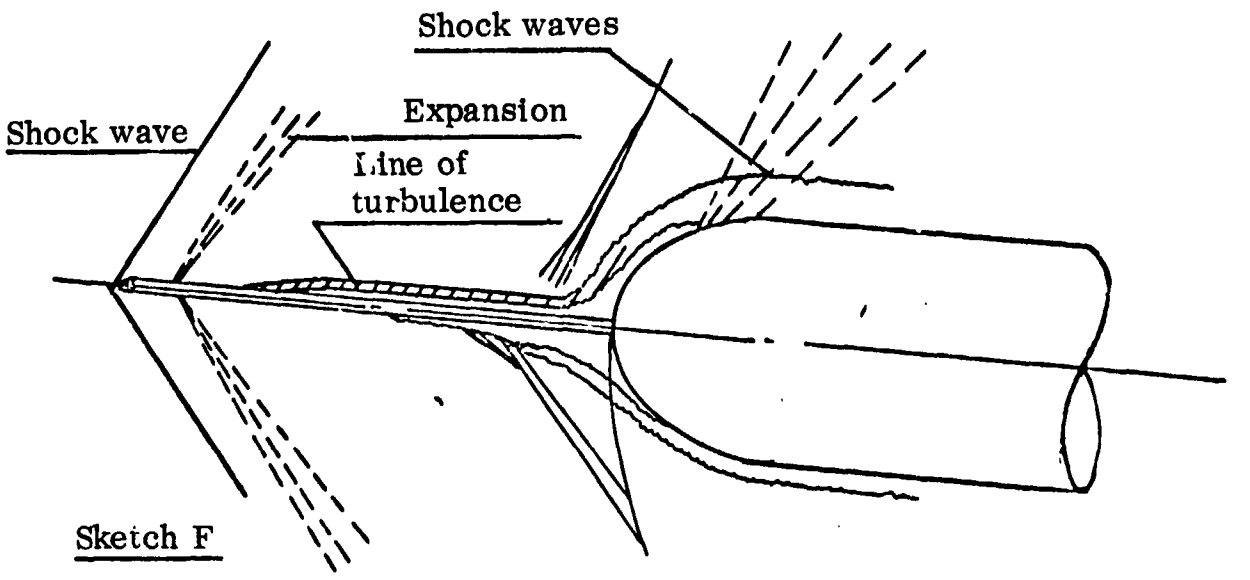

Sketch F

VERY LONG SPIKE

6.3. Experiments at M = 1.5 and M = 2.25

/28

6.3.1. The Drag

It was established in our experiments that the rise in drag disappears at an angle of attack of 15°. Figures 20 and 21 compare data for blunt as compared with spiked bodies for two Mach numbers. *

6.3.2. The Lift and the Pitching Moment

For these a slight increase was apparent with spiked configurations as compared with blunt bodies. In Figs. 22 - 25 the lift and the pitching moment coefficients appear as a function of angle of attack for spiked configurations and for blunt bodies. This increase is evident at both Mach numbers.

6.3.3. Center of Pressure

Computations of the center of pressure show that its location did not shift in spiked configurations as compared with blunt nosed bodies. In Figs. 26 and 27 x_{cp}/D appears as a function of angle of attach α. The change in the center of pressure is almost linear with α.

---

*A jump in drag was not found for nonzero angles of attack. For different spike lengths the decrease in resistance caused by the spike disappears with an increase in the angle of attack, because the detached zone no longer shields the hemisphere, and because the ratio of the drag on the hemisphere to the drag on the entire body is small.

CHAPTER 7

CRITERIA FOR THE USE OF SPIKES /29

We now consider the conditions under which it is advantageous to use a spike. We consider the problem in two distinct parts:

a. Mach number range and [blunt body] geometry.

b. Range of angles of attack.

7.1. Range of Mach Numbers and [Blunt Body] Geometry

The principle of the spike's operation consists in replacing the detached wave by system of conic waves, as illustrated by the following sketch:

The feasibility of using a spike is now determined by examining Fig. 1, where the drag curves for blunt bodies are plotted. Let us choose as an example the curve with $1f/R = 1.5$ and construct a new graph containing drag curves of cones with different vertex angles (see Fig. 28). It is evident from this figure that the curves of drag coefficient as a function of the free-flow Mach number exhibit different behavior for cones and blunt bodies. The drag of blunt bodies increases with increasing Mach number whereas the drag of the cones decreases. This means that under certain conditions the system of the conical wave system is "stronger" than the detached shock.

The drag coefficient of turbulent configurations is similar to that of the blunt configurations.

Hence the expedience of using a spike is determined by: /30

a. The geometry nose body.

b. The Mach number.

Spiking offers the greatest advantages in very blunt configurations and at high Mach numbers.

7.2. The Drag as a Function of the Flow Pattern in the Separated Boundary Layer

Let us consider now the experiments at Mach numbers 1.5 and 2.25 with configurations having 1f/R = 1.5.

M = 1.5

At this Mach number the conical wave system is "stronger" than the original shock itself, and therefore no appreciable drag reduction is obtained with a spike, as explained above.

M = 2.25

At this Mach number one gets a "classic" graph (see sketch G), which shows that there exists an optimal configuration, for which the resistance coefficient is minimal.

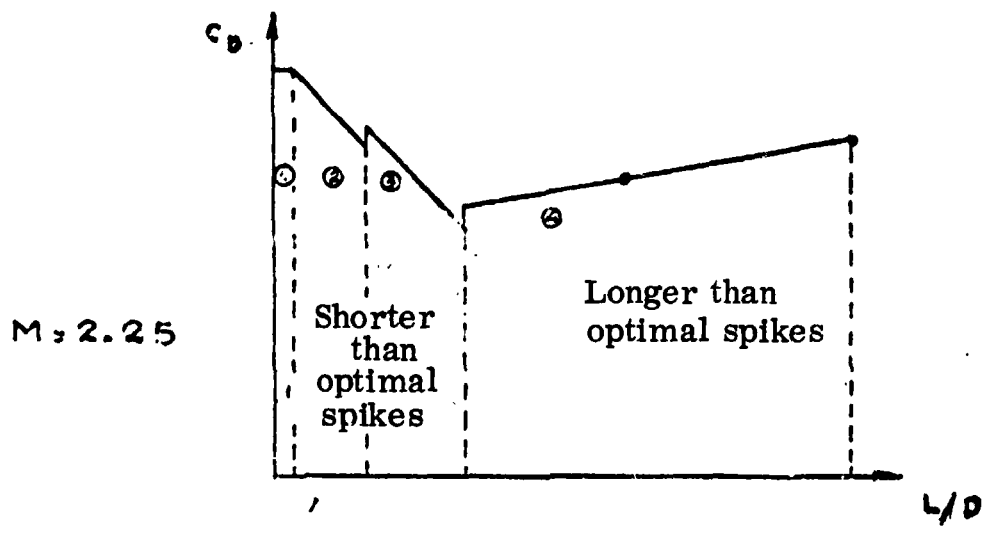

Let us see how departure from the optimal configuration increases the drag: /31

a. If a shorter-than-optimal spike is chosen: the angle of standing water becomes larger, which increases the drag coefficient.

b. With a larger-than-optimal spike the separation becomes turbulent, and again the angle of standing water becomes larger and the drag will increase with it, but in both cases the drag is less than its corresponding value for a blunt body without a spike.

The graph may be subdivided into four regions:

Region 1.: Region of constant C_D corresponding to the value of coefficient of a blunt configuration. The boundary of this region is the instant when the spike comes into contact with the detached shock with the attendant radical change in the flow pattern [9] gives the distance from the detached shock to the blunt nose body as function of Mach number. It is evident that this region is larger for smaller Mach numbers.

Region 2.: In this region the drag coefficient is variable (it usually decreases, but for certain configurations and at low Mach numbers it is liable to increase). At the points we have examined, a decrease was evident. This decrease is due to an increase in the fineness ratio of the standing-water zone.

Region 3.: Shifting of the separation point of the boundary layer from the spike tip to its shoulder, is accompanied by a sharp rise in drag. Subsequently it decreases continuously (it is assumed that the boundary layer is laminar) until an optimal L/D is reached for a certain combination of M and Re. Elongating the spike beyond the critical value will cause a jump in the drag as described in the sketch.

Region 4.: In this region the drag coefficient increases due to transition from laminar to turbulent flow in the mixing layer. The boundary layer is separating from spike body. The flow pattern remains unchanged and there is nc change in the drag coefficient. /32

7.3. Range of Angles of Attack

The purpose of spiking was to lessen the drag of blunt configurations. To the extent that these configurations are designed for high maneuverability including situations of very large angles of attack, there is no advantage in equipping them with spikes.

It was established in the present work and in former studies that the drag reduction obtained at zero angle of attack disappears at angle of attack of 15°. This explains why the use of spikes is limited to certain craft.

CHAPTER 8

/33

CONCLUSIONS

a. The drag of blunt bodies can be reduced by the equipping of their noses with a spike. The boundary layer separates upstream of the hemisphere and produces a conical flow pattern which shields the body.

b. The ratio of spike's length to the hemisphere radius is the important parameter determining the reduction in drag. For the configurations used in the present work, the drag is at minimum when the spike length is at maximum, i.e., that for which the flow is still separating from the spike's shoulder*.

The results below were checked in the range:

$$2 \times 10^5 < \mathrm{Ref} < 3 \times 10^6$$

$$1.5 < M < 2.75$$

1. When the flow is laminar and separating from spike's shoulder, the minimum separation angle is increasing with an increasing Re. This decreases the width of the detached cone, and with attendant reduction in the critical spike length.

2. The critical length increases with the increase in the ratio $a/2r_n$.

3. The drag reduction obtained at zero angle of attack becomes smaller with an increase in the latter angle until it disappears at an angle of approximately 15°.

4. The stability of the blunt body does not "deteriorate" with the installment of a spike. In most cases there is some improvement.

---

*Reference [22] did not consider these regions and, since the spikes used were relatively long (L/D = 2-3), it concludes that the drag coefficient decreases with an increase in spike's length, which is incorrect.

5. The critical length of a spike for certain conditions can be estimated from the following semi-empirical formula: /34

$$\frac{L}{2Rn} = \frac{1 - \sin\theta_c}{2\sin\theta_c} \left[1 + 2.5\left(\frac{d}{D}\right)^2 + 250\left(\frac{d}{D}\right)^4\right]$$

where:

$$\theta_c = \text{arc tg}\left[9.44\ (M^2 - 1)^{0.0917}\ (0.0592 - 0.012M)\ \frac{1}{1.69\sqrt{Re}^{0.0934}}\right]$$

6. For moderately blunt bodies (less than hemispherical) and at low supersonic Mach numbers, consideration should be given to the possibility that replacing the detached shock by a conical waves system may increase the drag, i.e., the drag coefficient under such conditions is greater than the coefficient of the blunt body.

7. If the boundary layer becomes turbulent before it reaches the spike's shoulder, then the separated-flow angle can be expected to become larger than in laminar flow. Therefore the drag will become greater and the critical length will be shorter.

Variations in Re will not greatly affect the separation angle, and when the critical spike length is passed there will be almost no change (or a very slight change) in the increase in drag.

REFERENCES

1) Data Sheets - Bodies 02.03.06.
R.A.S. 1960.

2) Flow Separation from Rods Ahead of Blunt Noses at Mach Number of 2.72.
NACA RM L52 E05 a, 1952.

3) Hart R.G.
Flight Investigations of the Drag of Round-Nosed Bodies of Revolution at Mach Numbers from o.6 to 1.5 using Racket Propelled Test Vehicles.
NACA RM L5IE25 1951.

4) Holder D.W., Chimeck A.
The Flow Past Elliptic-Nosed Cylinders and Bodies of Revolution in Supersonic Air Streams.
The Aeronautical Quarterly IV 317-340, 1954.

5) Chauvin L.T.
Pressure Distribution and Pressure Drag for a Hemispherical Nose at Mach Number 2.05, 2.54 and 3.04.
NACA RM L52K06, 1952.

6) Wallsko H.A., Hart R.G.
Investigation of the Drag of Blunt-Nosed Bodies of Revolution in free Flight at Mach Numbers from 0.6 to 2.3.
NACA RM L53D14 a. 1953.

7) Serbin H.
Supersonic Flow Around Blunt Bodies
J.A.S. Vol. 25, No. 1, 1958, pp. 58-59.

8) Eastman D.W., Radtke L.P.
Effect of Nose Bluntness on the Flow Around a Typical Ballistic Shape.
AIAA Journal Vol. 1, No. 10, 1963, pp. 2401-2402

9) Van Dyke, Milton
The Supersonic Blunt-Body Problem-Review and Extension
J.A.S.S. Vol. 25, No. 8, 1958, pp. 485-496.

References (Contd.)

10) Baer A.L.
Pressure Distribution on a Hemisphere Cylinder at Supersonic and Hypersonic Mach Numbers.
AEDC-TN-61-96 August 1961.

11) Gapcynski J.P., Robins W.
The Effect of Nose Radius and Shape on the Aerodynamic Characteristics of a Fuselage and Wing-Fuselage Combination at Angles of Attack.
NACA RM L53 I23 a, 1953.

12) Robins W.
Preliminary Investigation of the Effects of Several Seeker-Nose Configurations on the longitudinal Characteristics of a Canard-Type Missile at a Mach Number of 1.60.
NACA RM L53 I18, 1958.

13) Piland R.O.
Preliminary Free-Flight Investigation of the Zero-Lift Drag Penalities of Several Missile Nose Shapes for Infrared Seeking Devices.
NACA RM L52 F23, 1952.

14) Robinson R.B.
Aerodynamic Characteristics of Missile Configuration with Wings of Low Aspect Ratio for Various Combinations of Forebodies, Afterbodies and Nose Shapes for Combined Angles of Attack and Sideslip at a Mach Number of 2.01.
NACA RM L57 D19, 1957.

15) Walchner O.
Systematic Wind-Tunnel Measurements on Missiles.
NACA TM 1122, 1947.

16) Moeckel W.E.
Flow Separation Ahead of Blunt Bodies at Supersonic Speeds.
NACA TN 2418, 1951.

17) Moeckel W.E.
Flow Separation Ahead of a Blunt Axially Symmetric Body at Mach Numbers 1.76 to 2.10.
NACA RM E51125, 1951.

References (Contd.)

18) Mair W.A.
Experiments on Separation of Boundary Layers on Probes in Front of Blunt-Nosed Bodies in a Supersonic Air Stream
Phil. Mag. Vol. 43 No. 342, 1952 pp. 695-716.

19) Stalder J.R., Nelsen H.V.
Heat Transfer from a Hemisphere - Cylinder Equipped with Flow-Separation Spikes
NACA TN 3287, 1954.

20) Beastall D., Turner J.
The Effects of a Spike Protruding in Front of a Bluff Body at Supersonic Speeds
R & M No. 3007, 1952.

21) Hunt G.H.
Supersonic Wind-Tunnel Study of Reducing the Drag of a Bluff Body at Incidence by Means of a Spike
R.A.E. Report Aero 2606, 1958.

22) Kawasaki T.
Air Experimental Investigation about Spike Nose at Angle of Attack.
Proceedings from Congress of Applied Mechanics
Tokyo University 1966

23) Robinson M.L., Roberts B.G., Sayer A.M.
An Examination of the Flow Instability Associated with Spiked Bluff Body Configurations.
Australian Defence Scientific Service
Technical Note HSA 101. 1964.

24) Bogdonoff S.M., Vas E.I.
Preliminary Investigations of Spiked Bodies at Hypersonic Speeds.
JASS Vol. 26, No. 2, 1959 pp. 65-74.

References (Contd.)

25) Crawford D.H.
Investigation on the Flow Over a Spiked-Nose Hemisphere-Cylinder at a Mach Number of 6.8
NASA TN D-118, 1959.

26) Maull D.J.
Hypersonic Flow Over Axially Symmetric Spiked Bodies
Journal of Fluid Mechanics, Vol. 8, No. 4, 1969, pp. 584-592

27) Wood C.J.
Hypersonic Flow Over Spiked Cones.
Journal of Fluid Mechanics Vol.12, part 4, 1961, pp. 614-624.

28) Bogdonoff S.M., Vas I.E.
Some Experiments on Hypersonic Separated Flows
Archiwum Mechaniki Stosowanej, 1962, pp. 407-440.

29) Thurman N.E.
A Flow Separation Spike for Hypersonic Control of a Hemisphere-Cylinder.
AIAA Journal Vol. 2, No. 1, 1964, pp. 159-161.

30) Sims W.H., Boylan D.E., Jemy S.H.
Drag on Blunt Bodies with and without Spikes in Low-Density Hypersonic Flow.
AIAA Journal Vol. 3 No. 2, 1965, pp. 365-366.

31) Holden M.
Experimental Studies of Separated Flows at Hypersonic Speeds.
Part I: Separated Flows Over Axisymmetric Spiked Bodies
AIAA Journal Vol. No. 4, 1966, pp. 591-599.

32) Album H.H.
Regarding the Utility of Spiked Blunt Bodies
J. Spacecraft Vol. 5, No. 1, 1968, pp. 112-114.

33) הפקולטה להנדסה אוירונאוטית
רפר עזר למשתמש
. 1969

34) Donaldson C.d.P., Lange R.
Study of the Pressure Rise Across Shock Waves Required to Separate Laminar and Turbulent Boundary Layers.
NACA TN 2770, 1952.

References (Contd.)

35) Lubliner J., Oliver R.E., Morgan A.J.A.
Low to High Speed Drag Compilations for Rocket Test Slid Components.
NAVORD Report 5635.

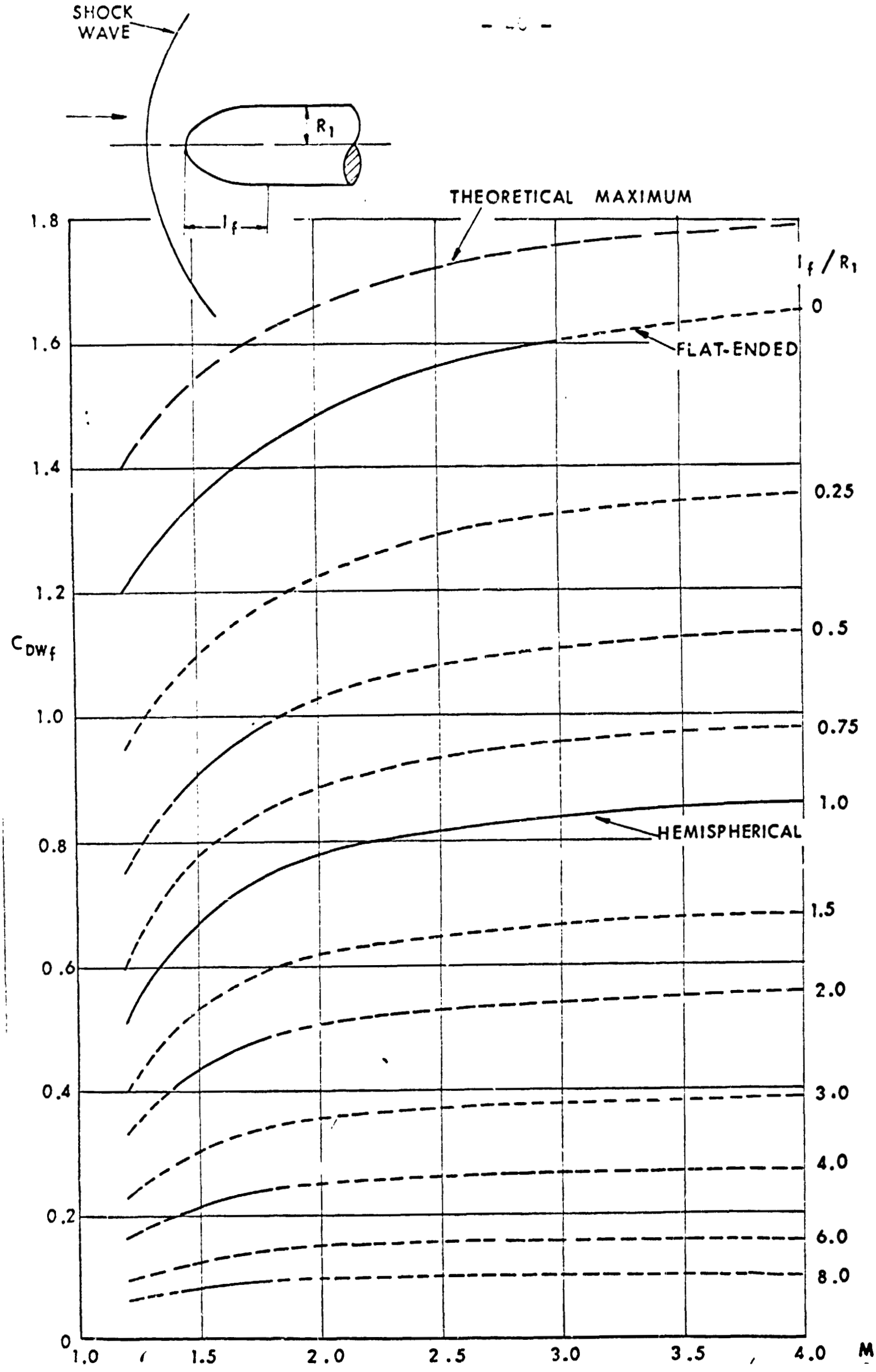

FIG. No. 1: WAVE DRAG OF BLUNT BODIES AS A FUNCTION OF M ACCORDING TO [1]

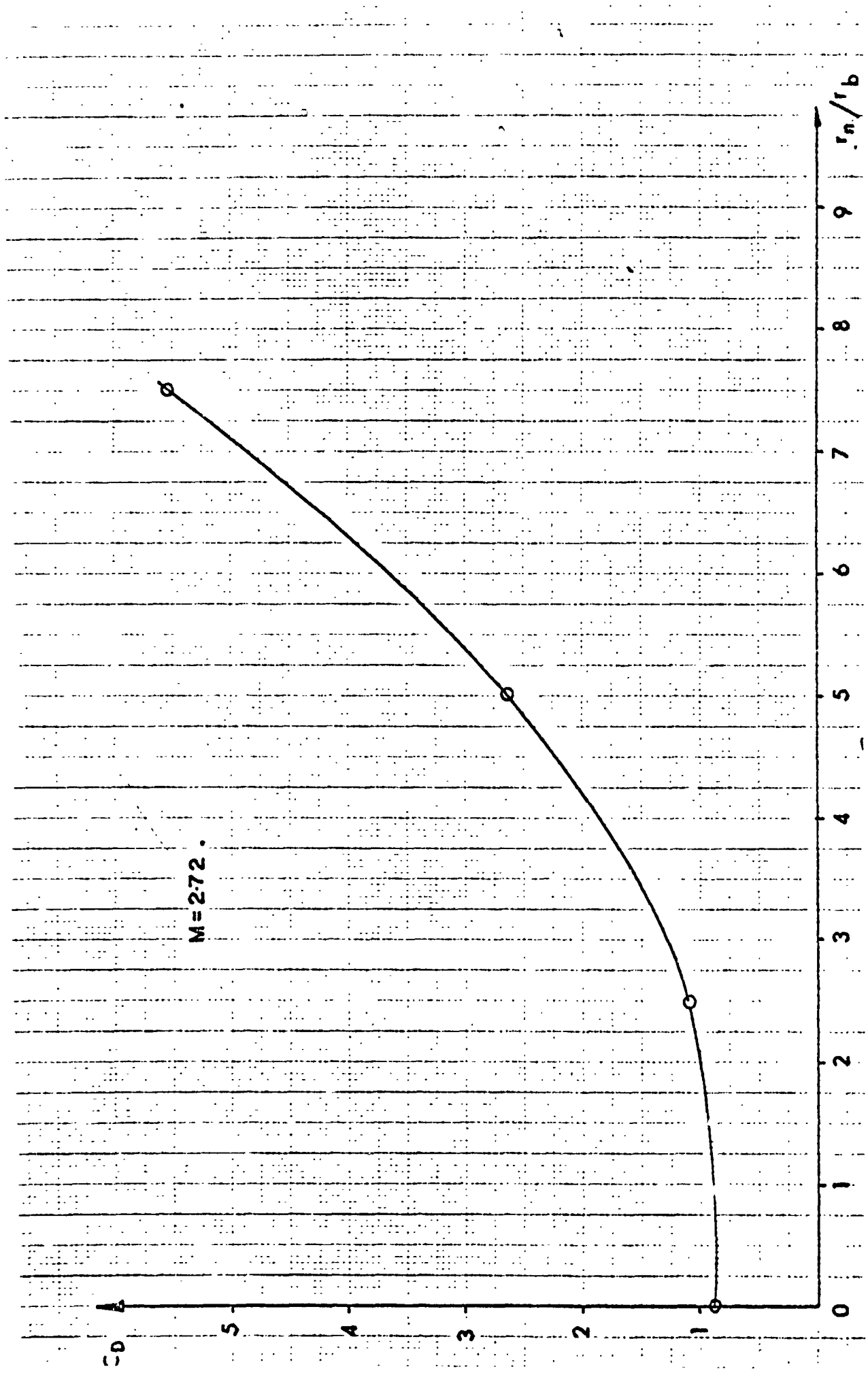

FIG. No. 2: EFFECT OF NOSE RADIUS ON DRAG COEFFICIENT

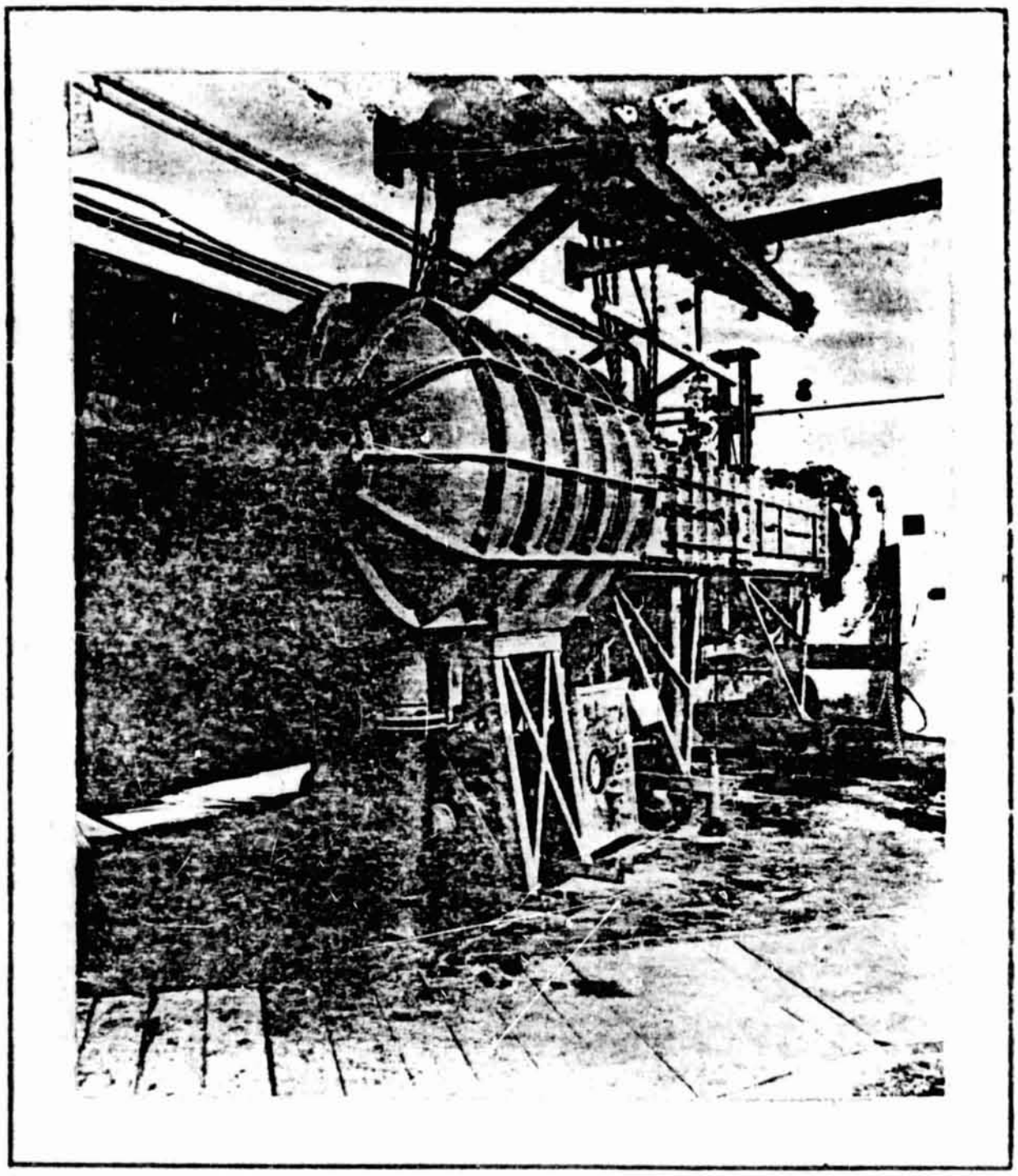

FIG. No 3: PICTURE OF No. 7. WIND TUNNEL

ציור מס' 3 : תמונת נקבת רוח מס' 7.

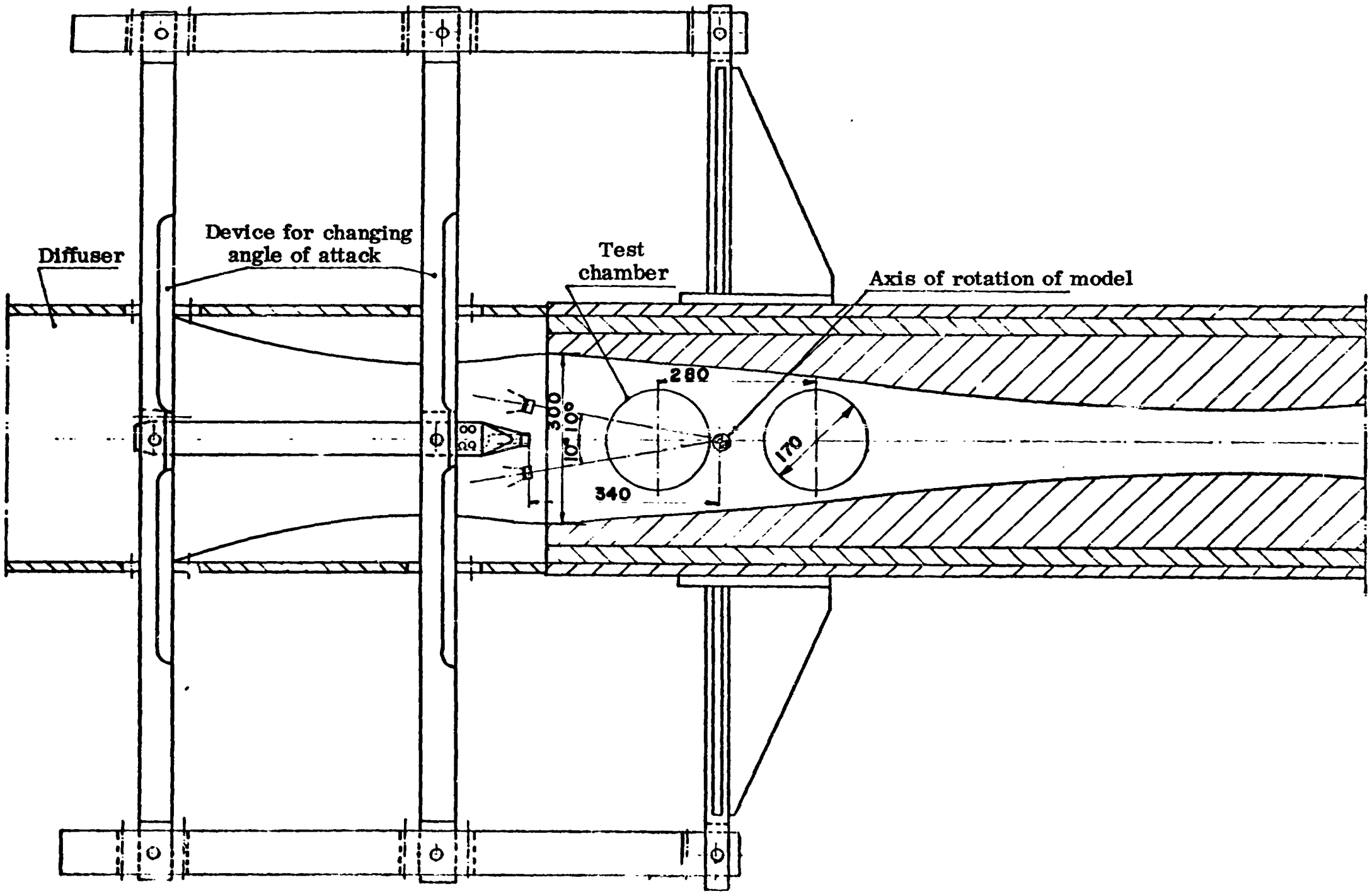

FIG. No. 4: TEST SECTION AND NOZZLE OF WIND-TUNNEL. No. 7.
ציור מס' 4 : נתיר וחא נסוי ניקבת רוח מס'7.

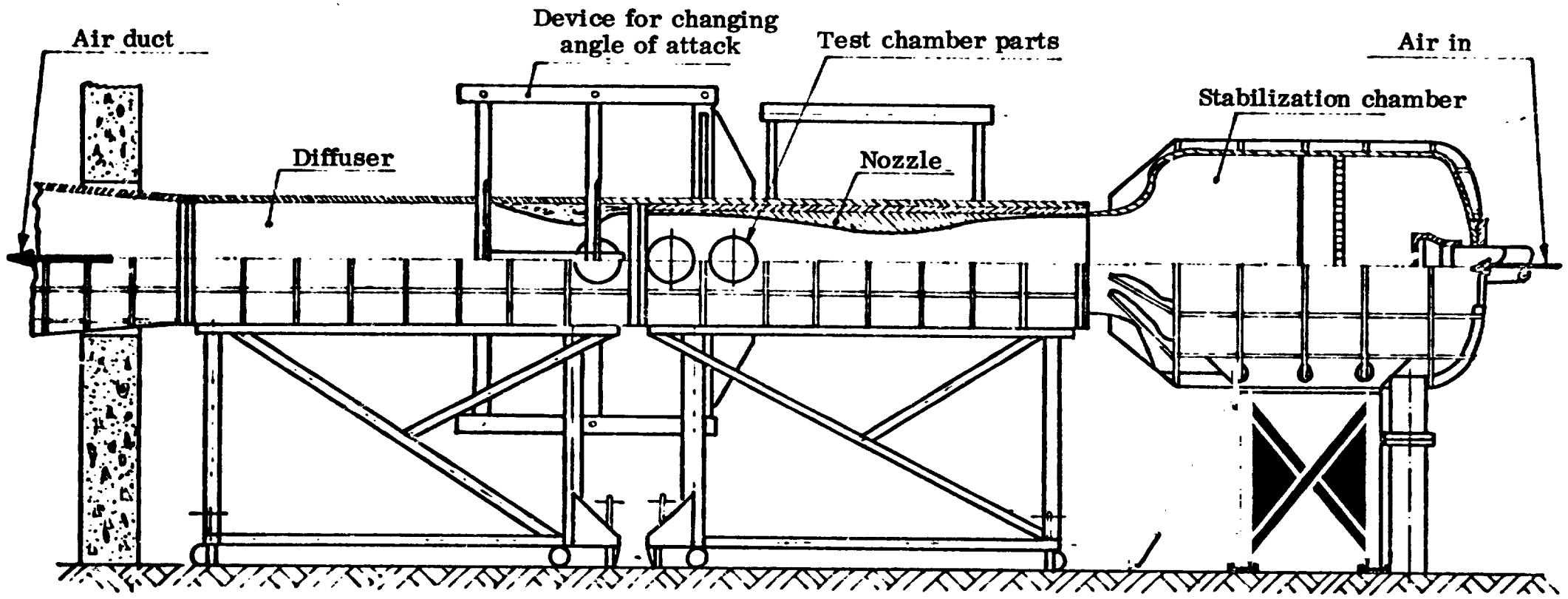

FIG. No. 5 : GENERAL VIEW OF WIND TUNNEL No. 7 .

ציור מס' 5: מראה כללי של נקבת רוח מס' 7 .

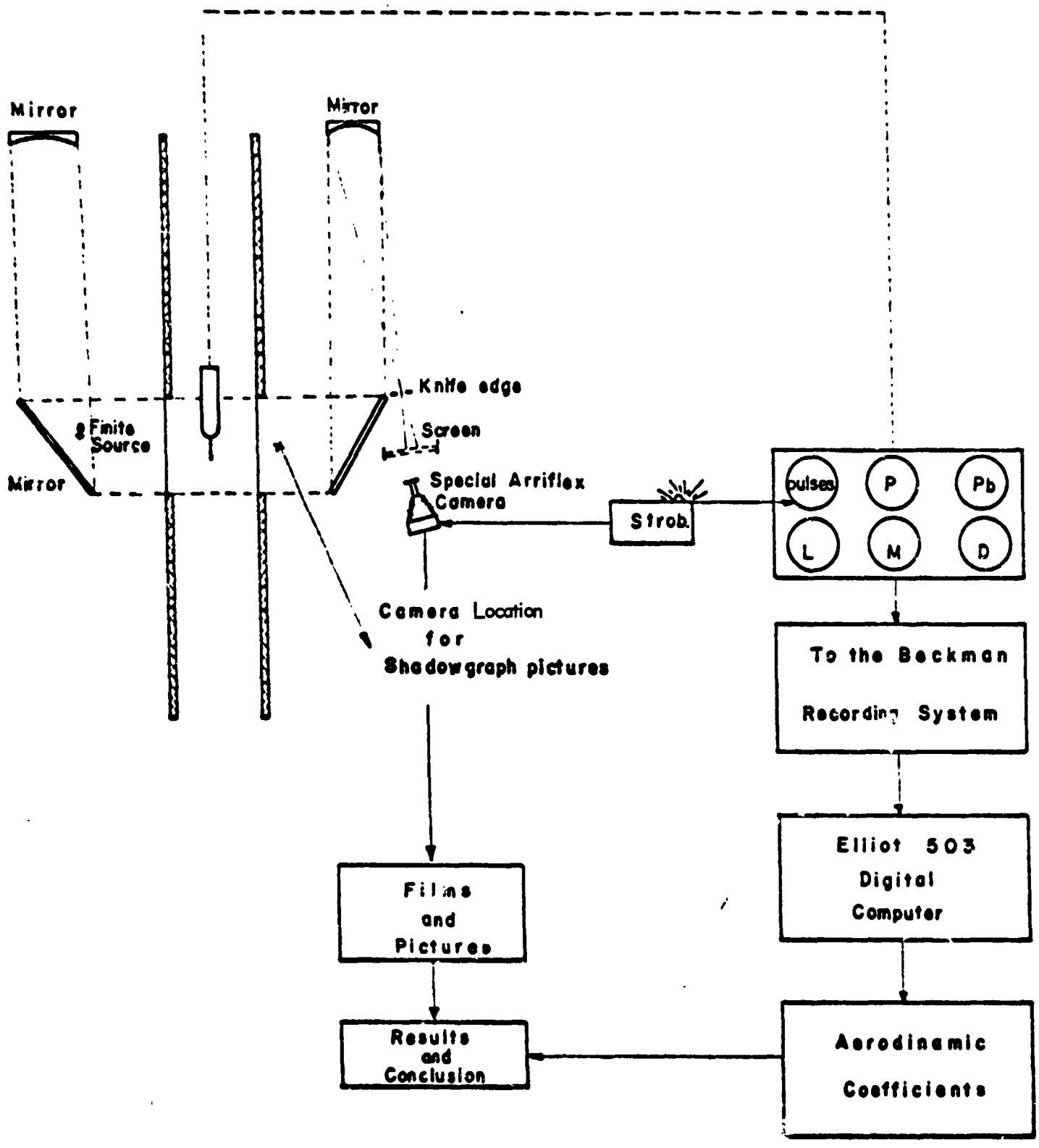

FIG. No. 6: APPARATUS AND EXPERIMENTAL TECHNIQUE.

ציור מס' 6: מכשור וטכניקת הנסוי.

37.

"O" דגם – MODEL "O".

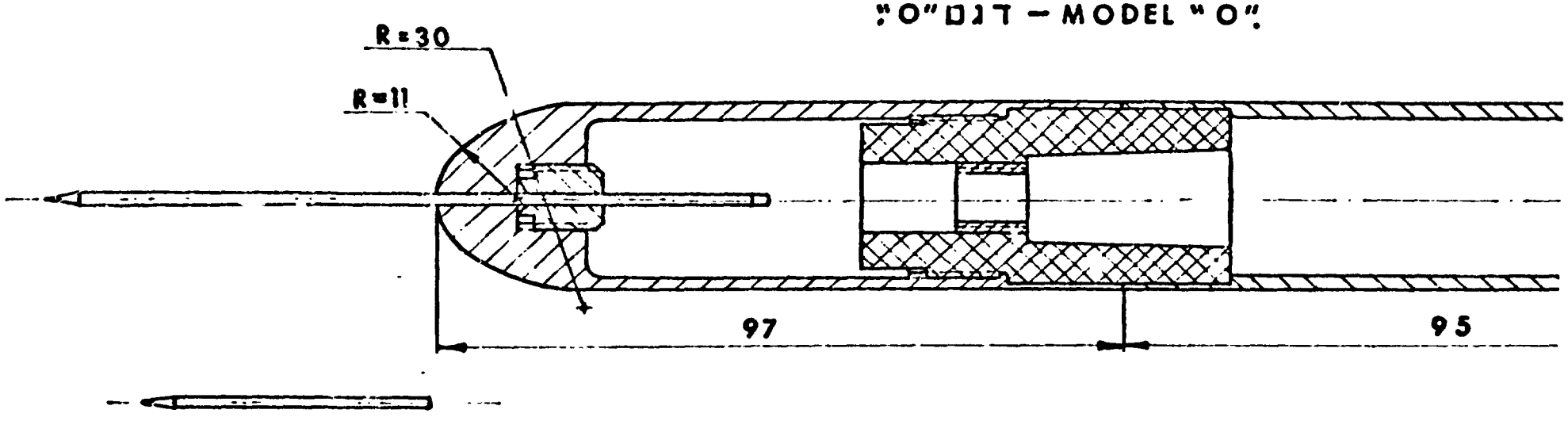

2.

1.5.

1.0.

"H" דגם – MODEL "H".

D=0.5.

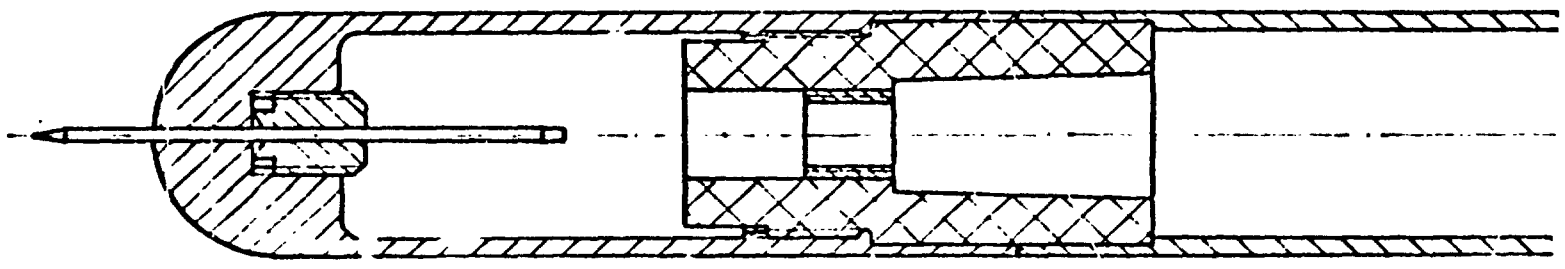

FIG.No.7: THE MODELS.
ציור מס' 7: הדגמים.

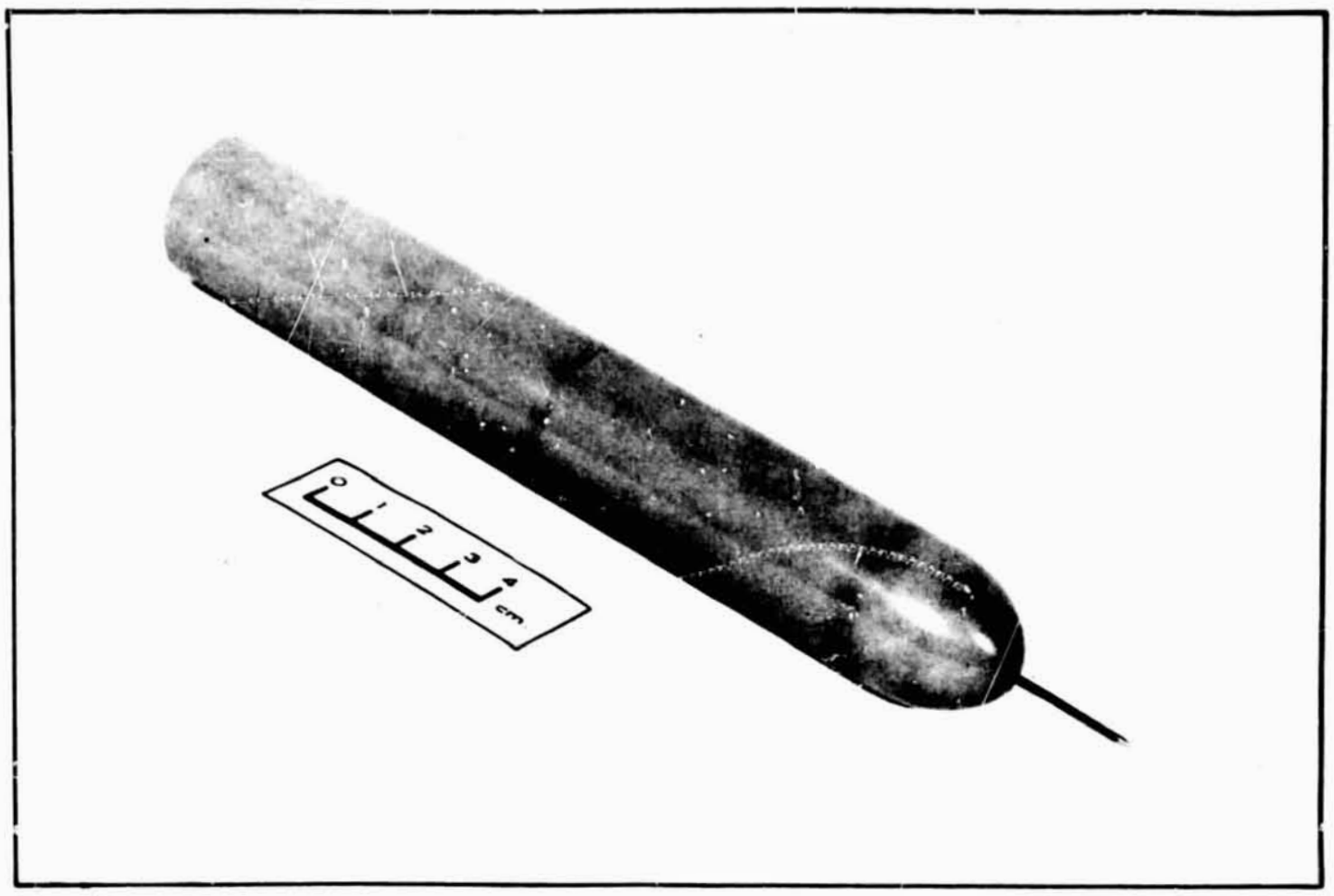

A. Ogive Model.

א. דגם אוגיב.

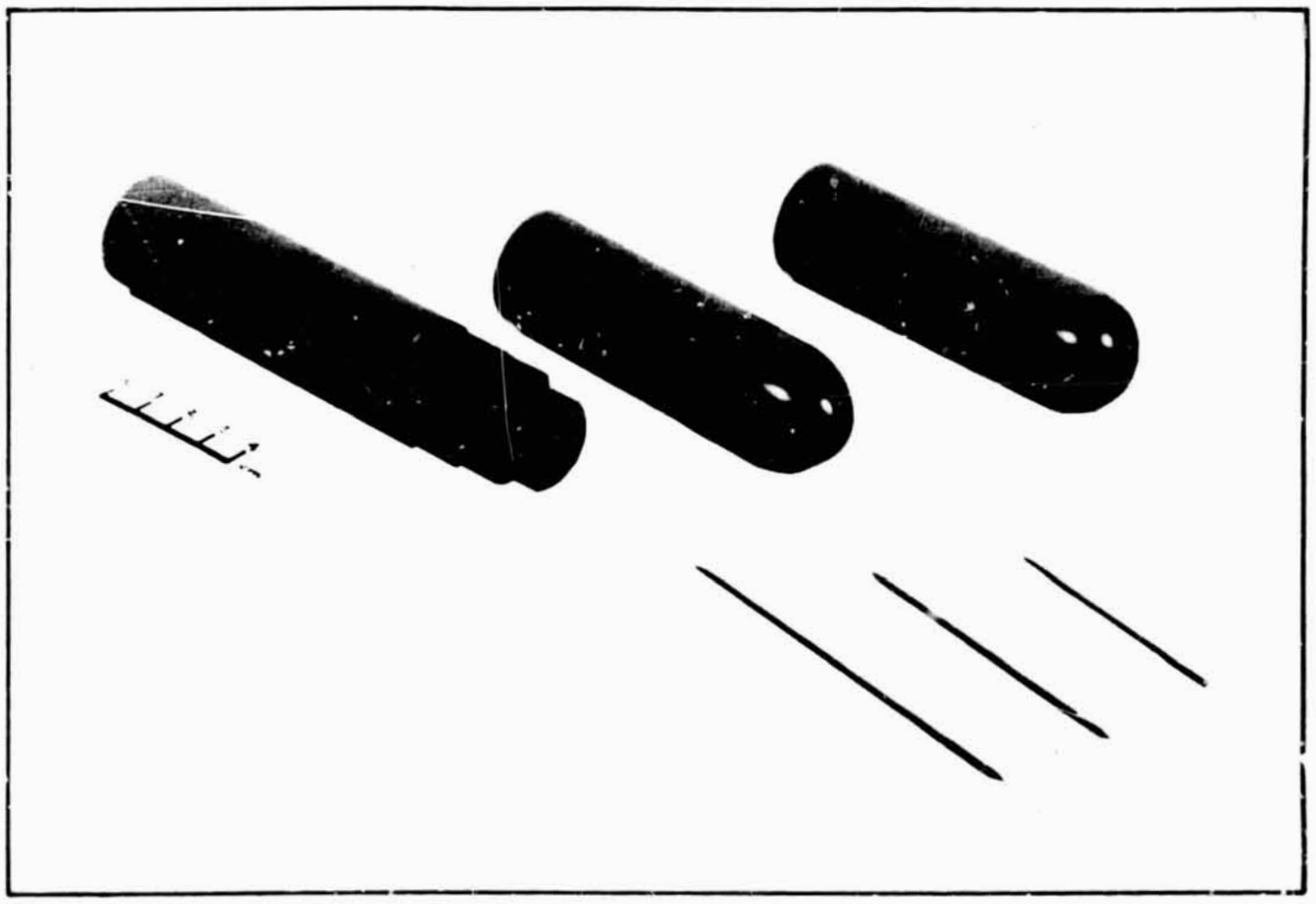

B. Noses spikes and after body. ב. הראשים, חודים והגוף האחורי.

FIG. No. 8: PHOTOGRAPHS OF MODELS

ציור מס' 8: תמונות הדגמים.

A

UNSTABLE FLOW DETACHED
FROM SPIKES SHOULDER

א

נתוק לא יציב מכתף החוד.

B

SEPARATION POINT MOVES DOWN-
STREAM.
THE CRITICAL LENGTH IS OBTAIN-
ED.

ב

נקודת הנתוק זזה אחורה.
הושג כך אזור האורך הקריטי.

C

SEPARATION POINT MOVES BACK
TO SPIKE'S SHOULDER.

ג

נקודת הנתוק חוזרת לכתף החוד.

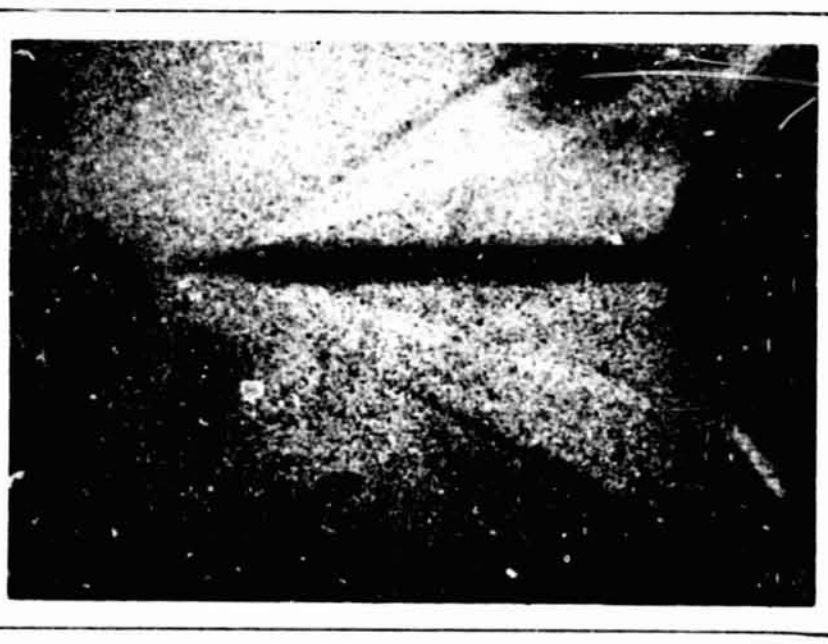

Experiment 651 '10J
L/D = 1. M = 2.25. $Re_D \cong 9 \times 10^5$.

FIG. No. 9: FLOW SENSITIVITY AT THE CRITICAL LENGTH ATTENDANT TO PRESSURE INCREASE.

M=2.25.

L/D = 0.5.

Re= $4 \times 10^{6} \frac{1}{(cm)}$.

FIG.No.10: JUMP OF DETACHED WAVE FROM SPIKE APEX TO SPIKE'S SHOULDER.

ציור מס' 10: קפיצת הגל המנותק מקודקוד החוד לכתף על' עלית הלחץ.

RUN 650 L/D = 0.5

RUN 649 L/D = 0

RUN 646 L/D = 2

RUN 651 L/D = 1

FIG.No.11: FLOW AT ZERO ANGLE OF ATTACK(M=2.25) SCHLIEREN AND SHADOW PICTURES.

RUN 752

$Re/cm = 5.10^5$ D = 0.5

RUN 753

$Re/cm = 4.8 \times 10^5$ L/D = 1

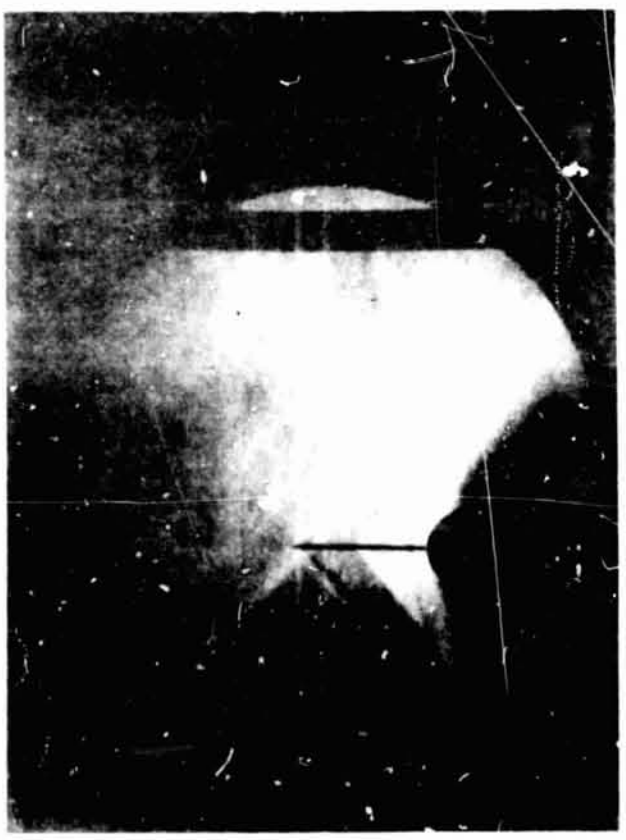

RUN 754

$Re/cm = 5.3 \times 10^5$

L/D = 1.5

FIG. No. 12: FLOW AT ZERO ANGLE OF ATTACK(M =1.5) SCHLIEREN PICTURES.

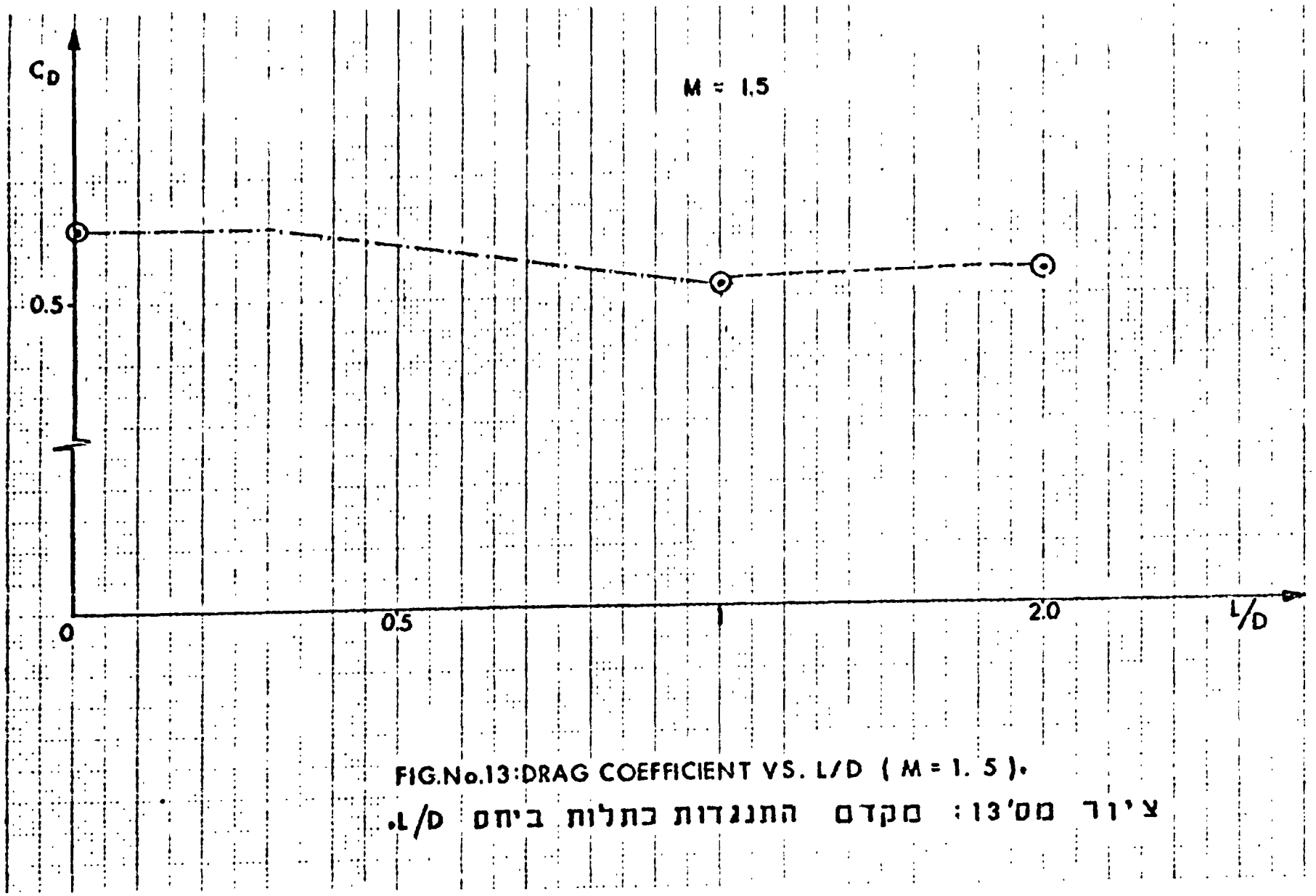

FIG.No.13:DRAG COEFFICIENT VS. L/D (M = 1. 5).

ציור מס'13: מקדם התנגדות כתלות ביחס L/D.

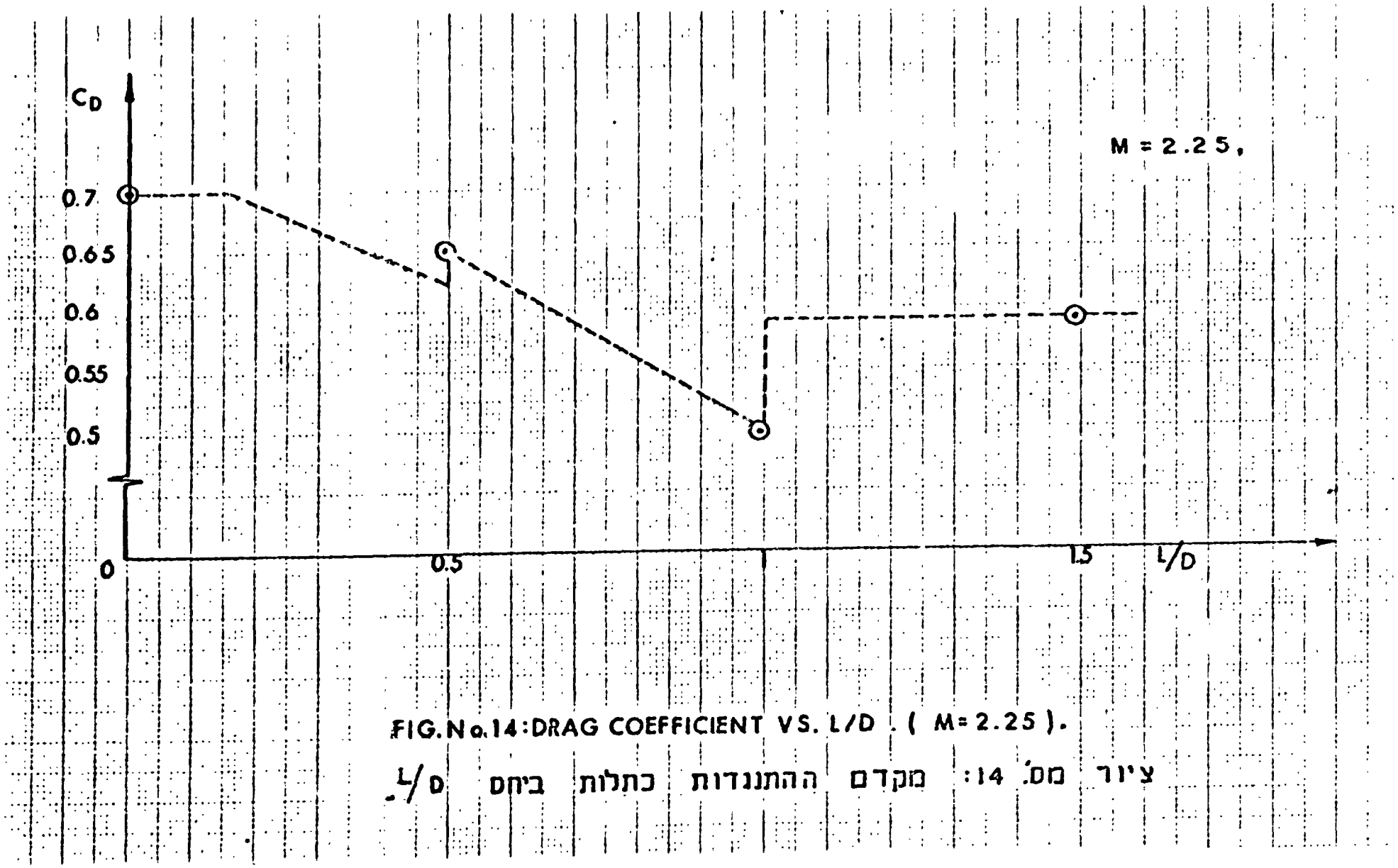

FIG.No.14:DRAG COEFFICIENT VS. L/D . (M=2.25).

ציור מס. 14: מקדם ההתנגדות כתלות ביחס L/D.

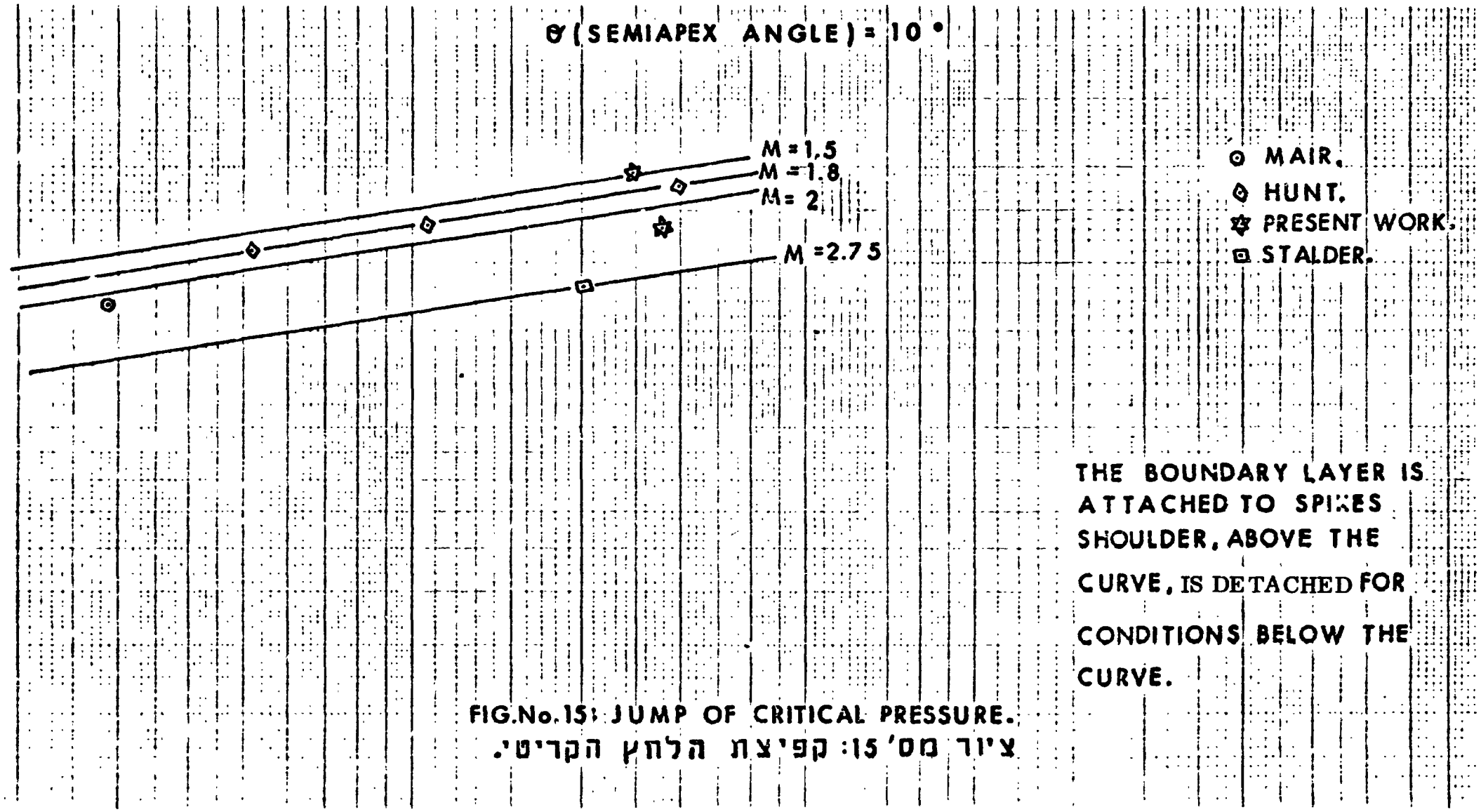

FIG.No.15: JUMP OF CRITICAL PRESSURE.

ציור מס' 15: קפיצת הלחץ הקריטי.

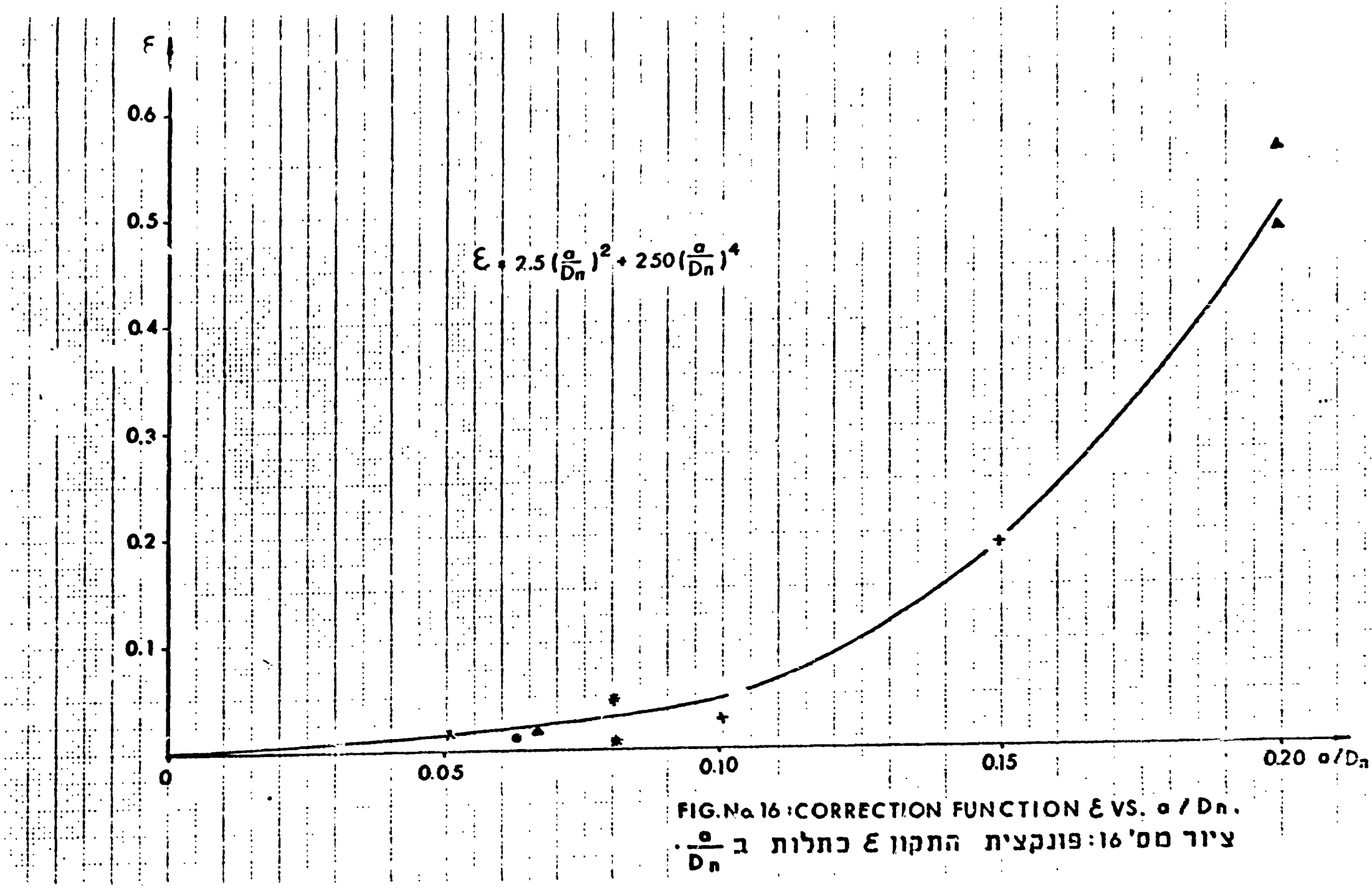

FIG.No 16 : CORRECTION FUNCTION ε VS. a / Dn .

ציור מס' 16: פונקצית התקון ε כתלות ב $\frac{a}{D_n}$.

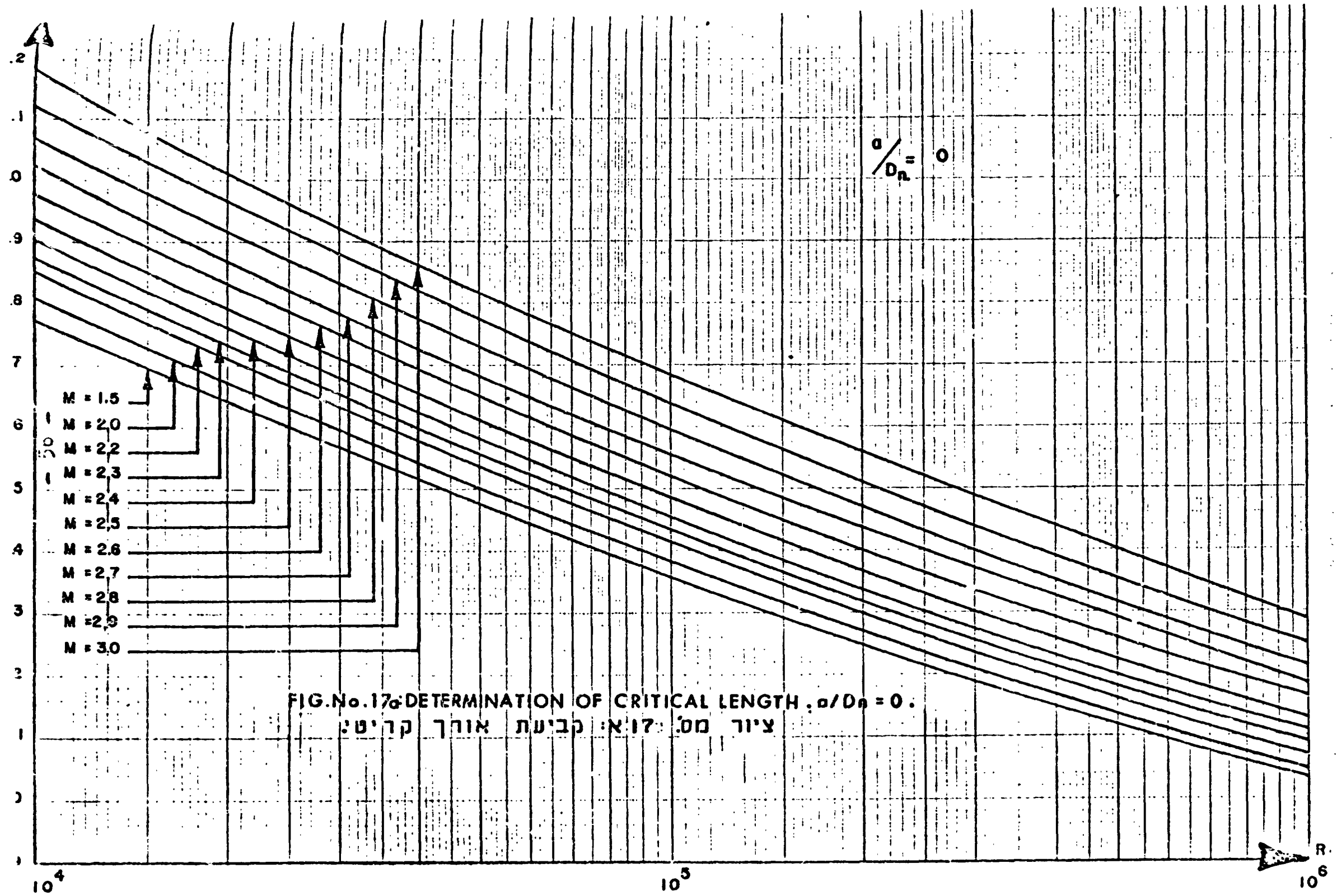

FIG.No.17a DETERMINATION OF CRITICAL LENGTH , a/Dn = 0 .

ציור מס' 17א: קביעת אורך קריטי.

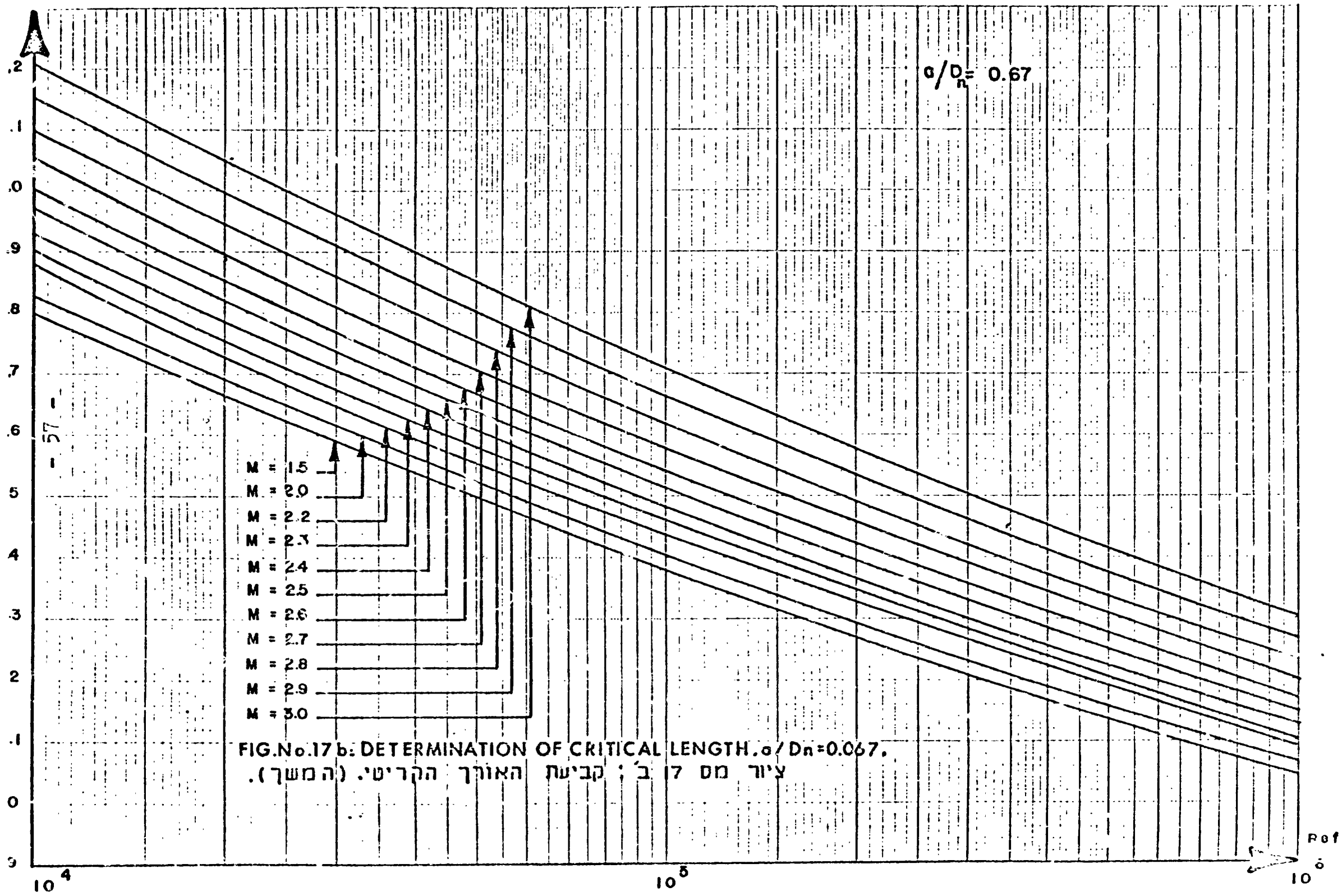

FIG.No.17 b: DETERMINATION OF CRITICAL LENGTH. a/Dn=0.067.

ציור מס 17 ב' ; קביעת האורך הקריטי. (המשך).

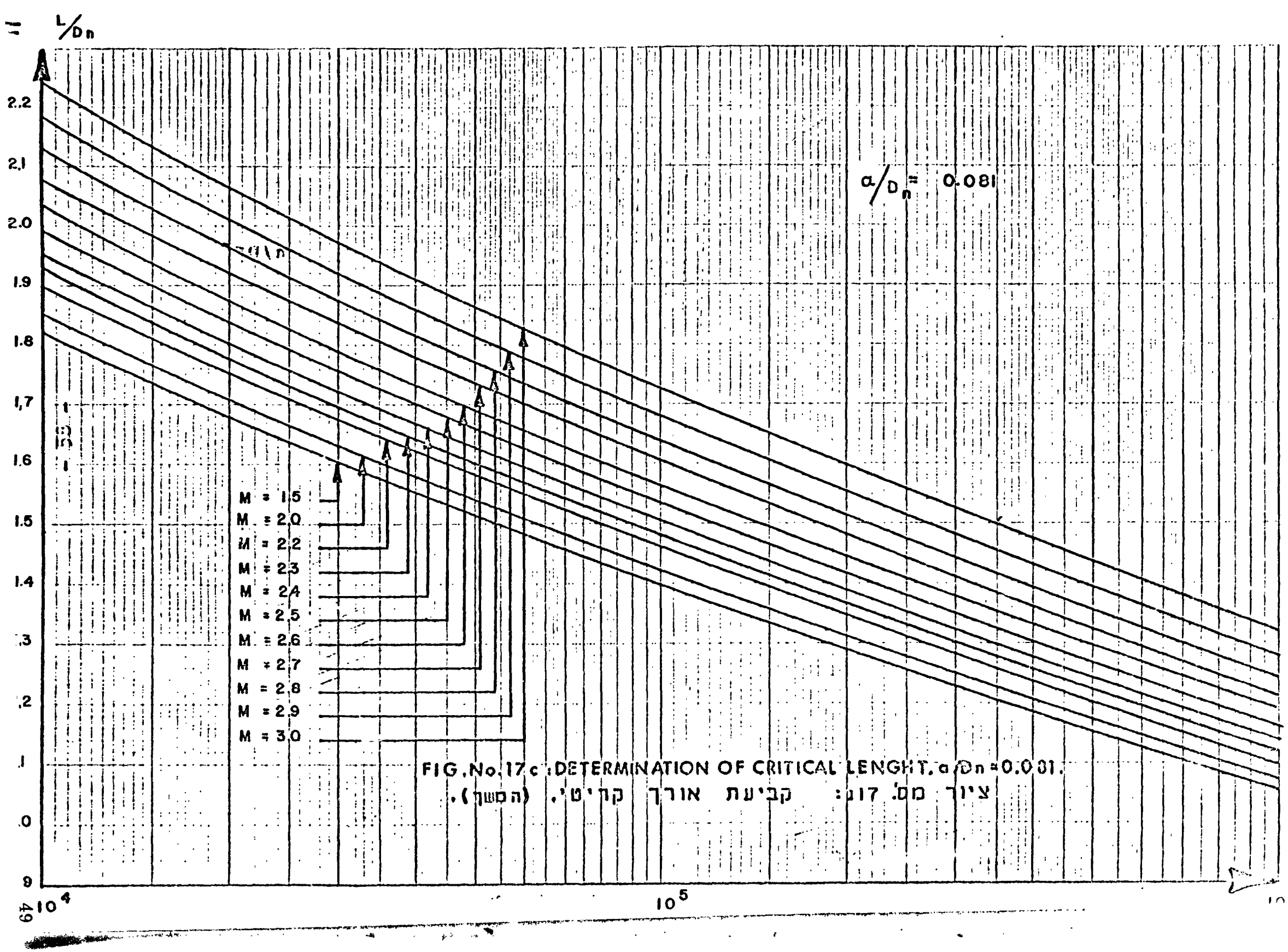

FIG. No. 17c : DETERMINATION OF CRITICAL LENGHT. $\alpha/D_n = 0.081$.

ציור מס. 17ג: קביעת אורך קריטי. (המשך).

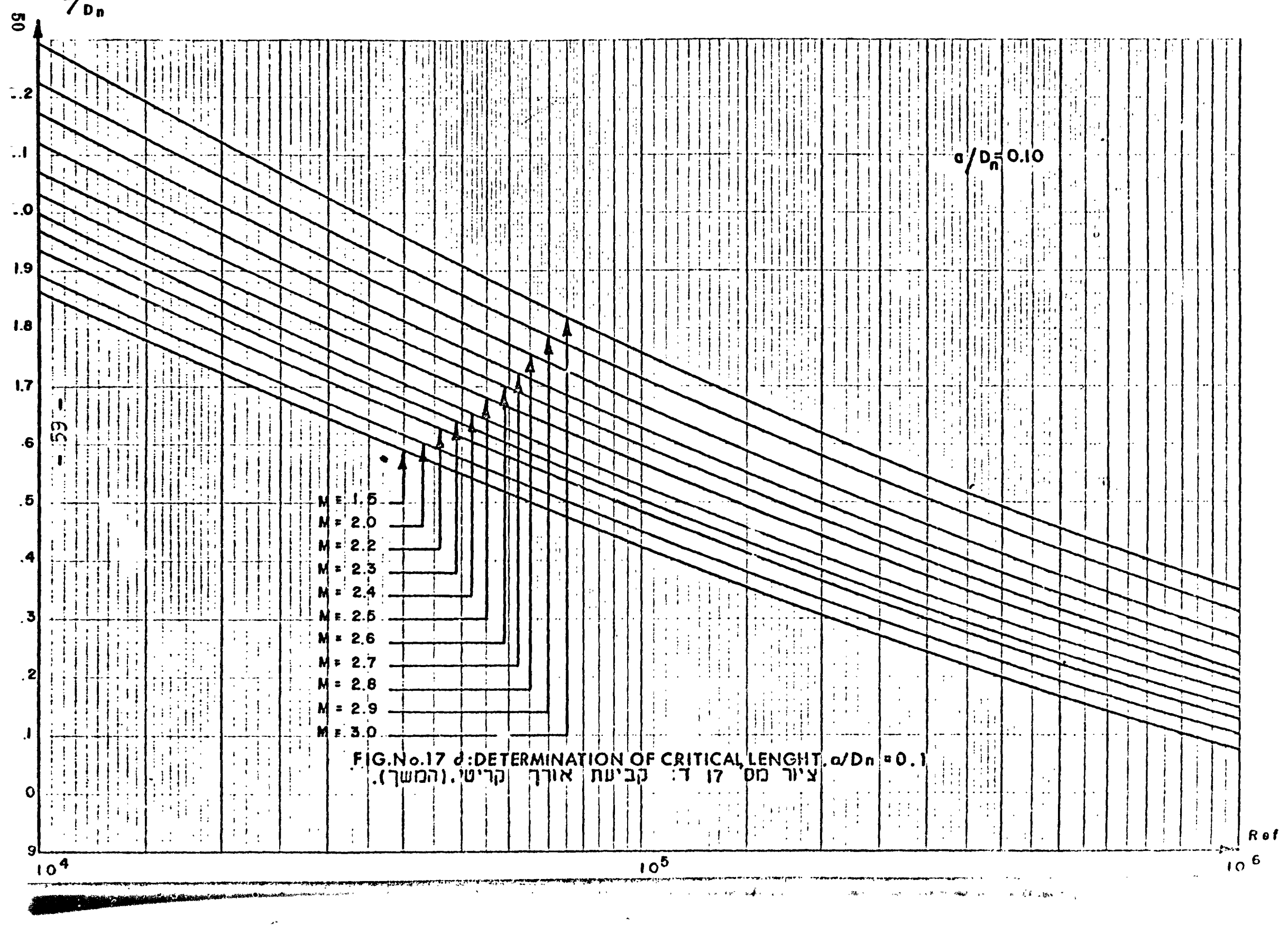

FIG.No.17 d:DETERMINATION OF CRITICAL LENGHT. a/Dn = 0.1

ציור מס' 17 ד: קביעת אורך קריטי.(המשך).

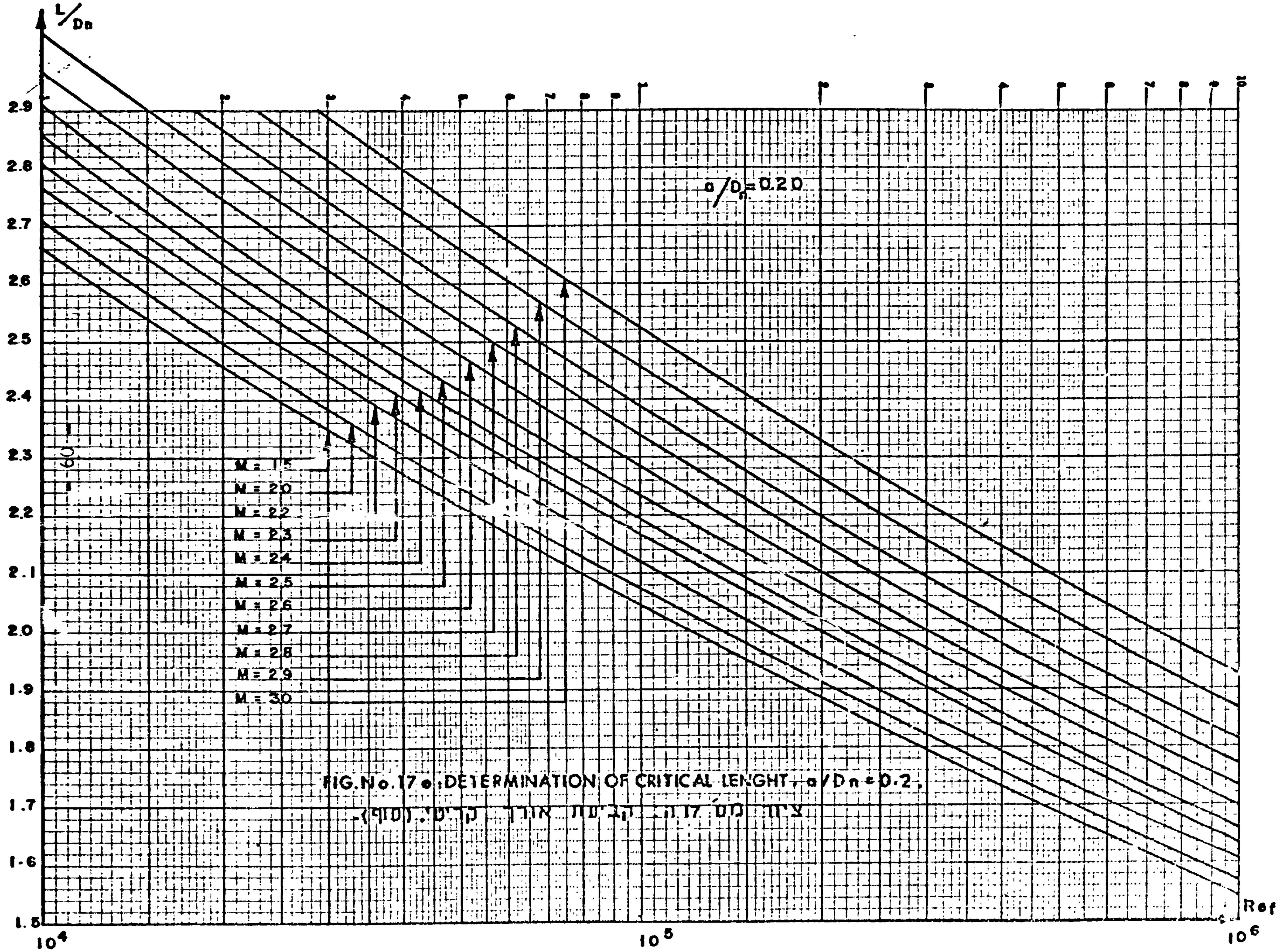

FIG. No. 17 e: DETERMINATION OF CRITICAL LENGHT, a/Dn = 0.2.

ציור מס' 17ה. קביעת אורך קריטי. (סוף).

RUN . 723

M = 2. 25.

Rod = 7×10^5

$\alpha = 6°30'$

$\alpha = 12°30'$

ציור מס'18: תצורה"ס"ללא חוד בזוית התקפה.(תצורה קהה)

FIG. 18: FLOW AT ANGLE OF ATTACK M=2.25. (BLUNT CONFIGURATION).

RUN .716

$\frac{L}{D}$= 0.5

$Re/_{cm} = 3 \times 10^5$

RUN .721

$\frac{L}{D}$=1.0

$Re/_{cm} = 3.8 \times 10^5$

ציור מס'19: זרימה בזוית התקפה M=2.25. (תצורות מחודדות).

FIG 19: FLOW AT ANGLE OF ATTACK M=2.25. (SPIKED CONFIGURATIONS).

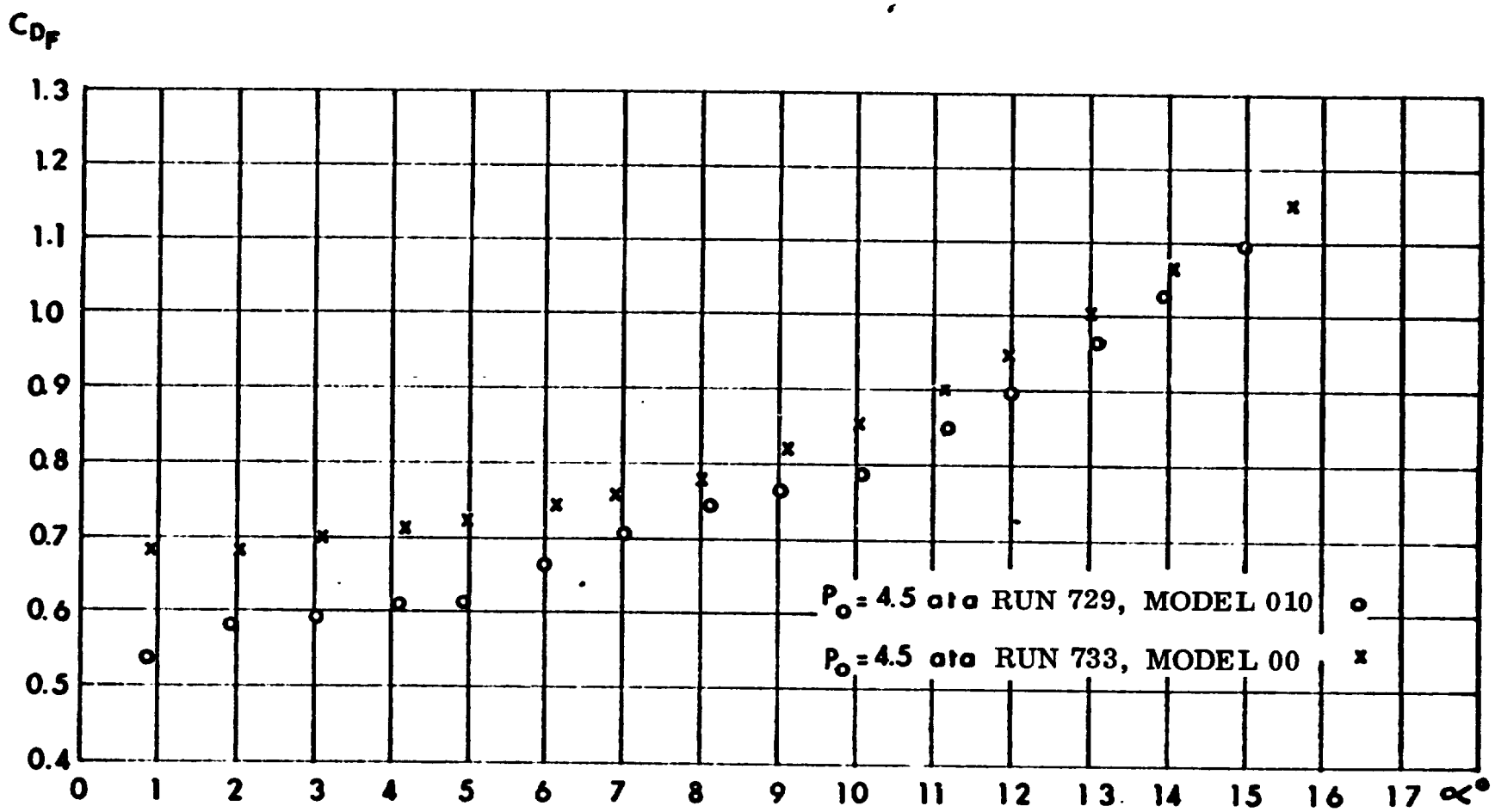

FIG. No. 20: DRAG COEFFICIENT OF CONFIGURATIONS 000 AND 010 VS. ANGLE OF ATTACK (M = 2.25).

ציור מס' 20 : מקדמי התנגדות הגל של תצורות 010,000 כתלות בזוית ההתקפה.(M = 2.25).

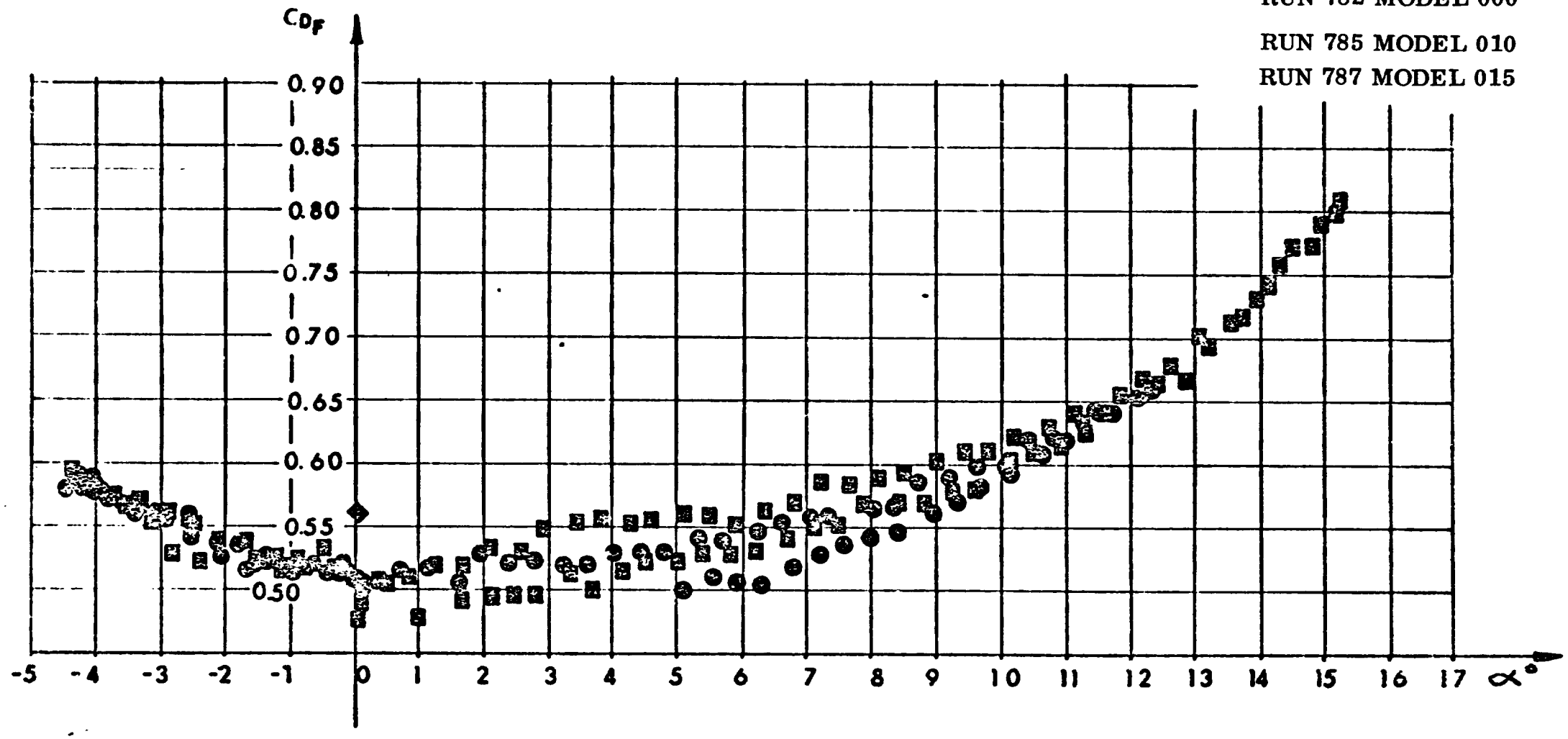

ציור מס' 21: מקדמי התנגדות הנר של התצורות 015,010 כתלות בזוית התקפה.
עבור התצורה 000, נתן מקדם ההתנגדות ב- $\alpha = 0^\circ$ בלבד.

FIG. No. 21: DRAG COEFFICIENT OF CONFIGURATIONS 000, 010 AND 015 VS. ANGLE OF ATTACK.
(M = 1.5) (The Drag Coefficient for Configuration 000 is Given Only at $\alpha = 0$).

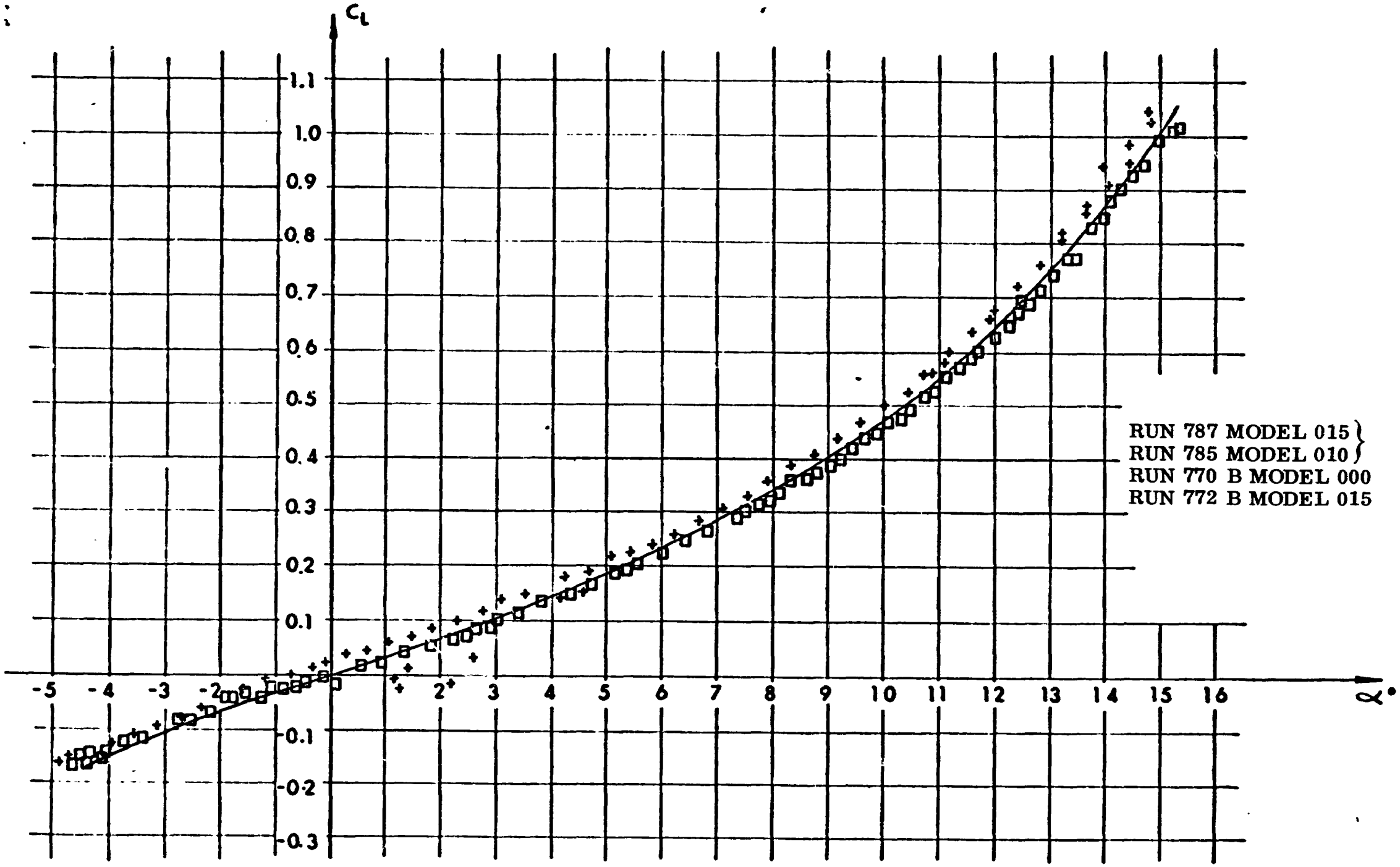

FIG. No.22 :LIFT COEFFICIENT OF 000,010 AND 015 CONFIGURATIONS VS. ANGLE OF ATTACK(M=1.5).
ציור מס' 22 : מקדמי העלוי של התצורות 015,010,000 כתלות בזוית התקפה.(M=1.5)

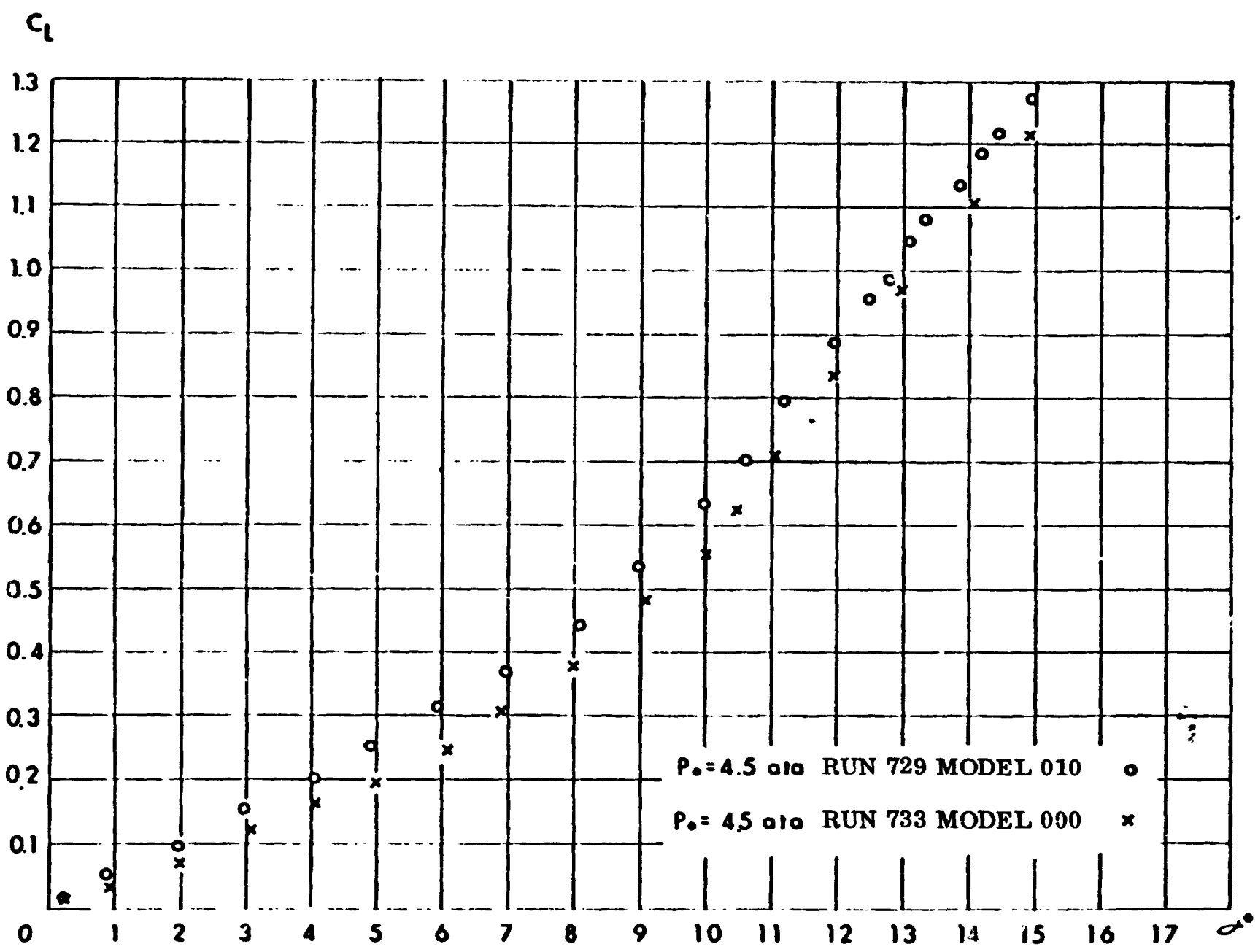

FIG. No. 23: LIFT COEFFICIENT OF 000, AND 010 CONFIGURATIONS VS. ANGLE OF ATTACK. (M = 2.25).

ציור מס' 23: מקדמי העלוי של התצורות 010,000 כתלות בזוית ההתקפה. (M=2.25).

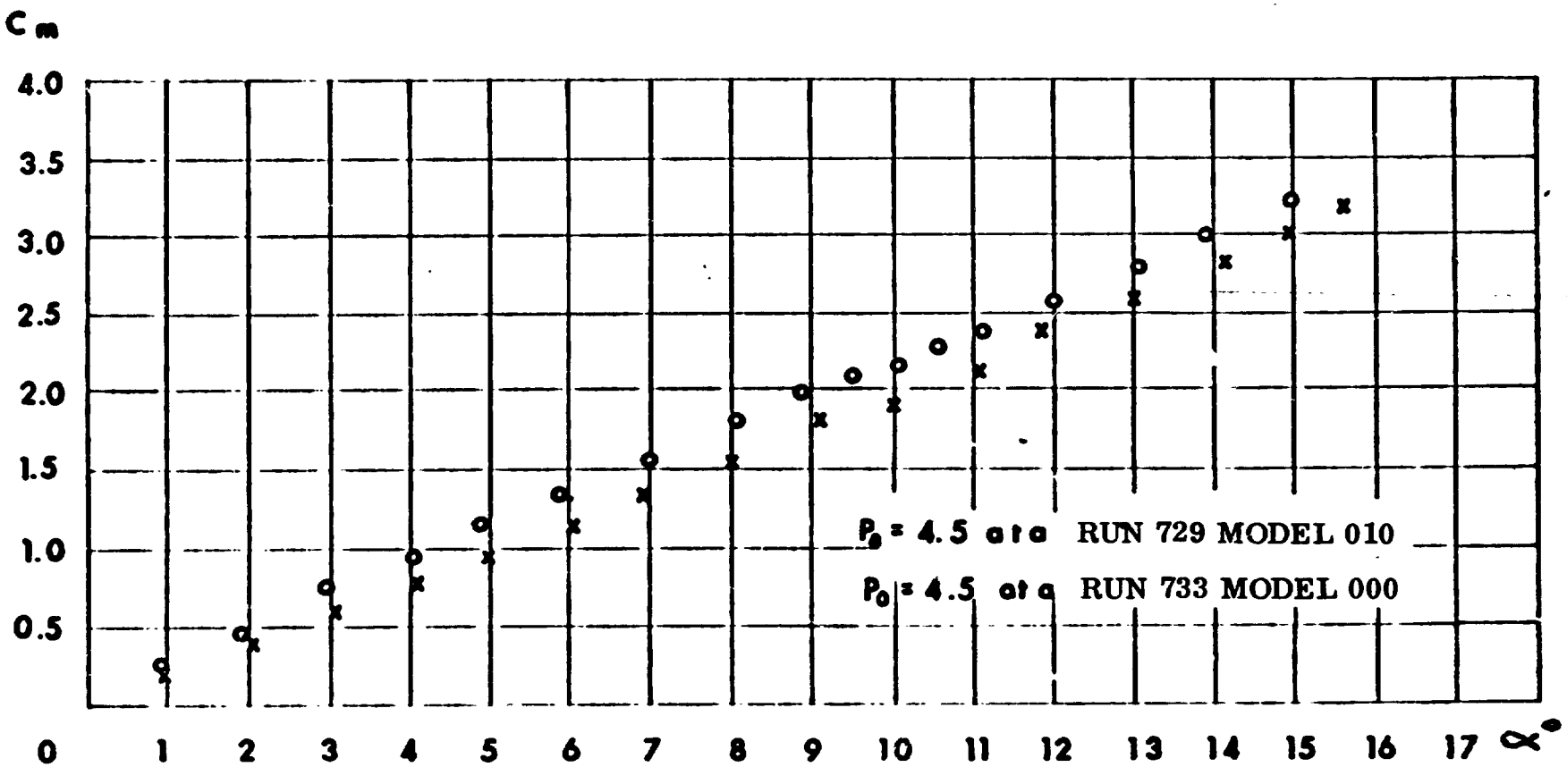

FIG. No. 24: PITCHING MOMENT COEFFICIENT OF 000 AND 010 CONFIGURATIONS VS. ANGLE OF ATTACK (M=2.25).

ציור מס' 24: מקדמי המומנט של התצורות 010,000 כתלות בזוית ההתקפה (M=2.25)

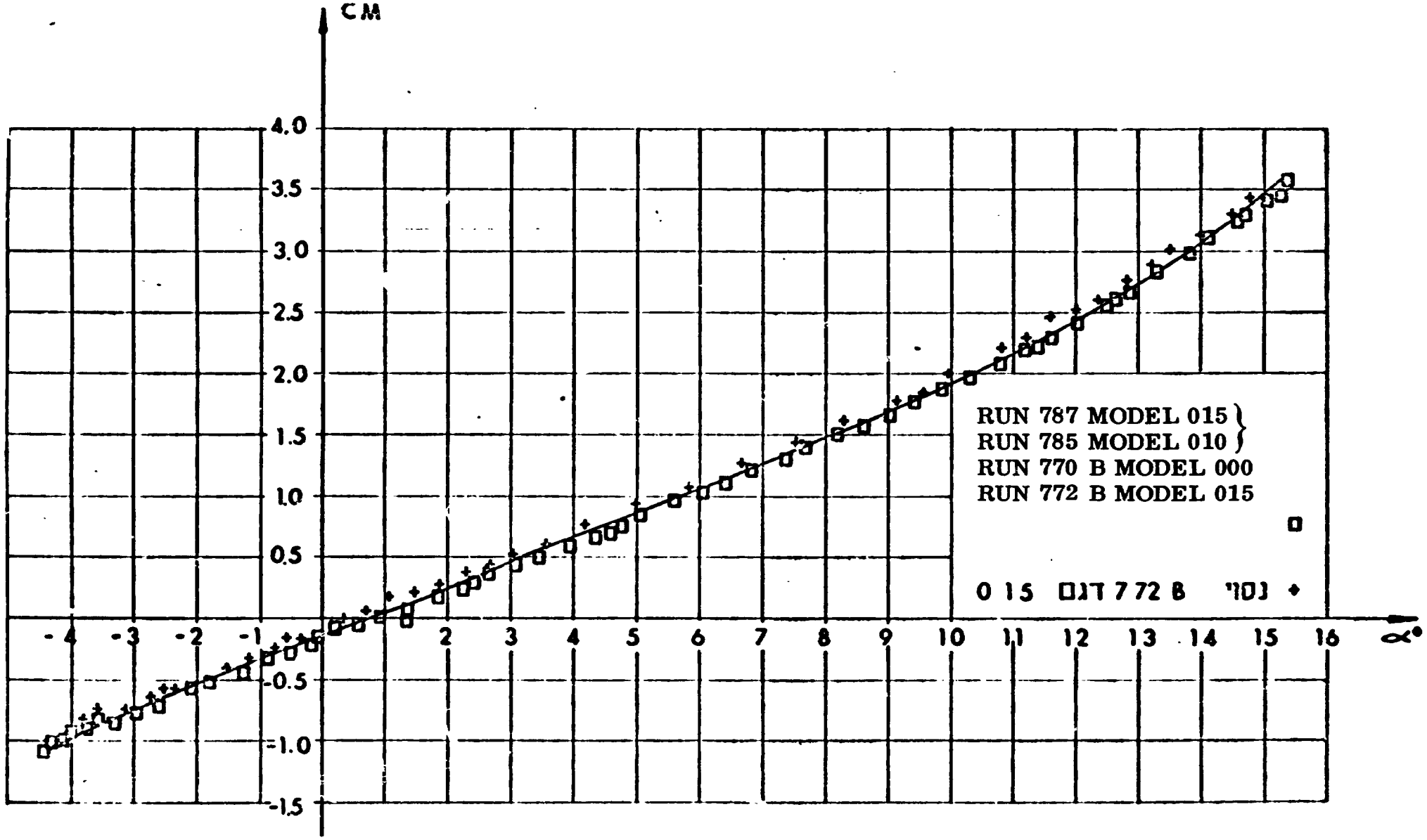

ציור מס' 25: מקדמי המומנט של התצורות 015,010,000 כתלות בזוית התקפה. (M =1.5).

FIG. No. 25: PITCHING MOMENT COEFFICIENT OF 000,010 AND 015 CONFIGURATIONS VS. ANGLE OF ATTACK (M = 1.5).

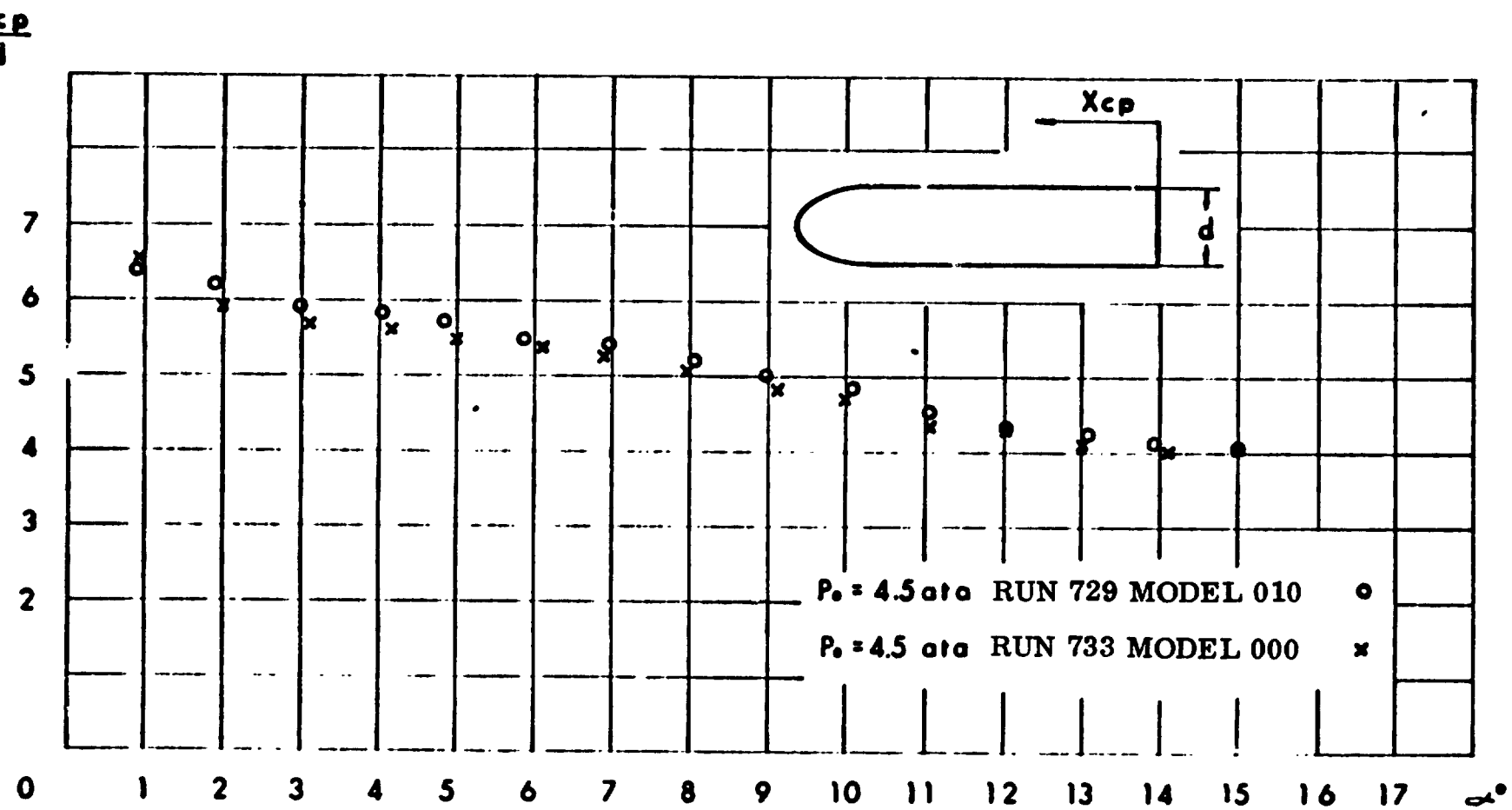

FIG.No. 26 :CENTER OF PRESSURE DISTANCE FOR 000 AND 010 CONFIGURATIONS VS. ANGLE OF ATTACK (M = 2.25).

ציור מס' 26 : מרחק מרכז הלחץ של 010,000 כתלות בזוית התקפה (M = 2.25).

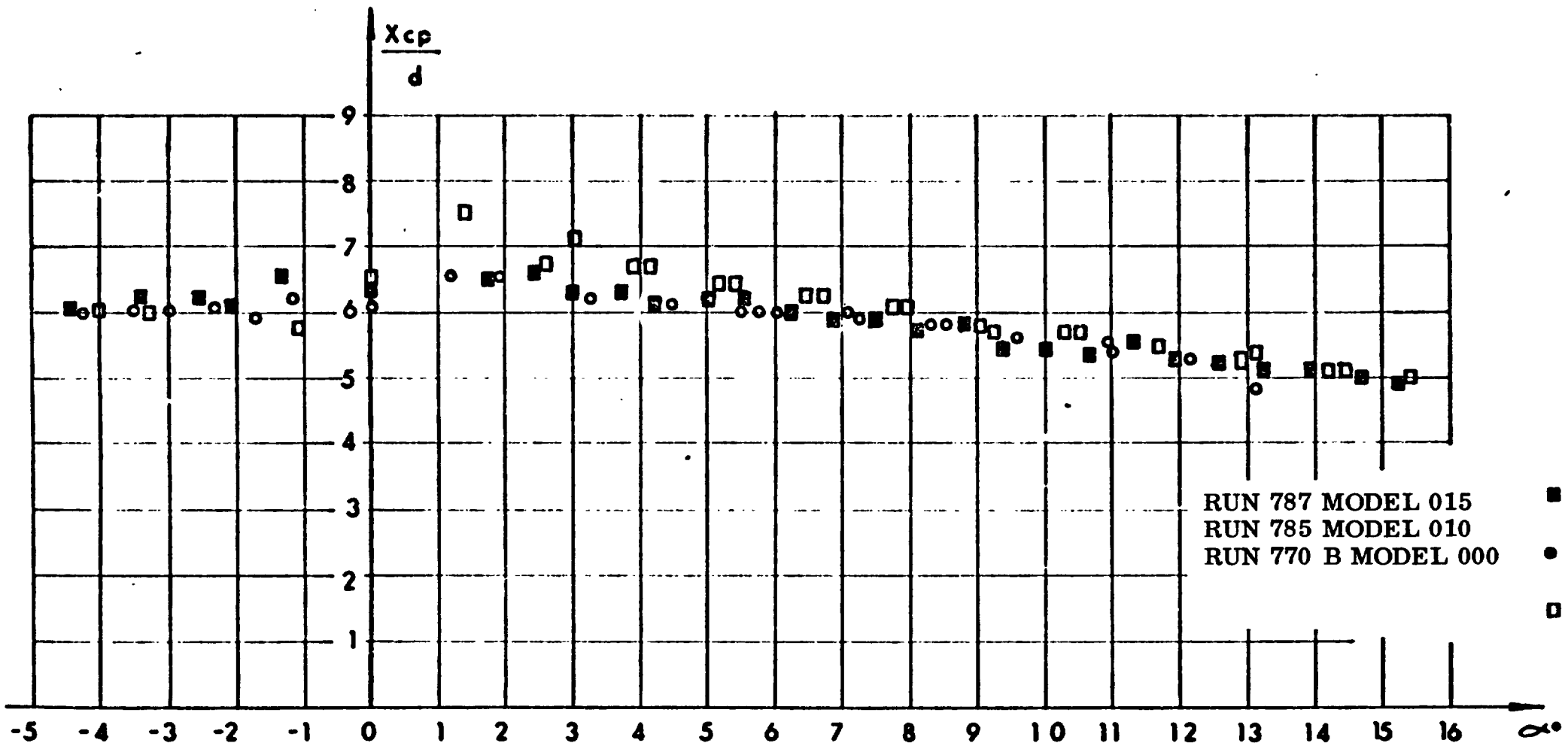

FIG. No. 27: CENTER OF PRESSURE DISTANCE FOR 000, 010 AND 015 CONFIGURATIONS VS. ANGLE OF ATTACK (M=2.25).

ציור מס' 27: מרחק מרכז הלחץ מבסיס הדגם של תצורות 015,010,000 כתלות
בזוית ההתקפה α. (M=1.5).

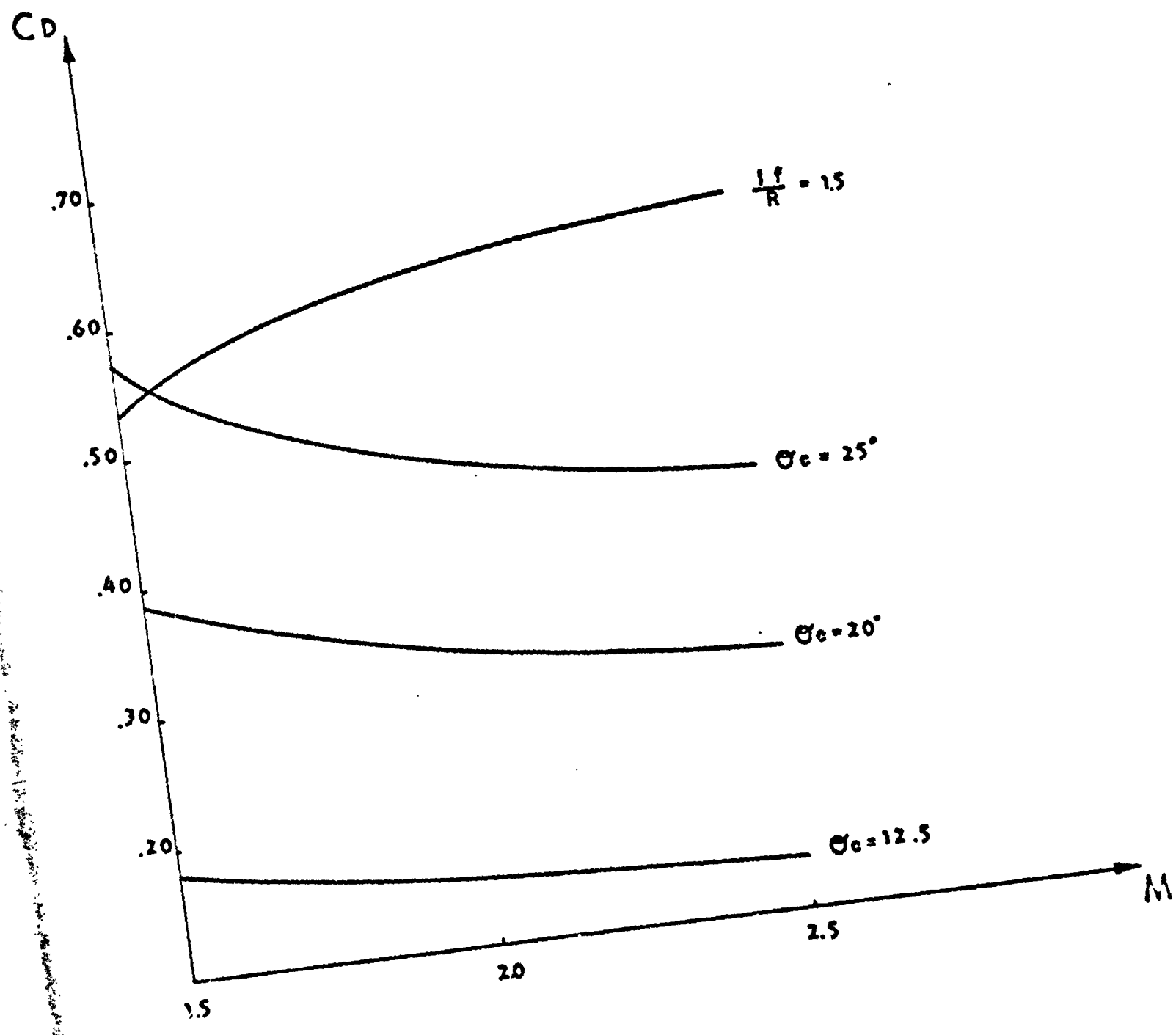

FIG. No. 28 :DRAG COEFFICIENT VS. MACH NUMBER FOR CONES AND BLUNT BODIES.

ציור מס' 28: מקדם התנגדות כתלות במס' מאך עבור נוף קהה וקונוסים.